SpezialForschungsBereich F 32

Karl–Franzens Universität Graz
Technische Universität Graz
Medizinische Universität Graz

An optimal control approach to the elastic/hyperelastic image registration problem

Marcus Wagner

SFB-Report No. 2010–031 August 2010

A–8010 GRAZ, HEINRICHSTRASSE 36, AUSTRIA

Supported by the
Austrian Science Fund (FWF)

SFB sponsors:

- **Austrian Science Fund** (FWF)
- **University of Graz**
- **Graz University of Technology**
- **Medical University of Graz**
- **Government of Styria**
- **City of Graz**

An optimal control approach to the elastic/hyperelastic image registration problem

Marcus Wagner

1. Introduction.

Among the basic tasks of mathematical image processing is the *image registration problem*:[01] Let us assume that two greyscale images are given, which will be described through functions $I_0(s)$, $I_1(s)\colon\ \Omega \to [\,0\,,\,1\,]$ on a rectangular domain $\Omega \subset \mathbb{R}^2$.[02] Considering I_0 as reference image, one wants to determine a vector field $x(s)\colon\ \Omega \to \mathbb{R}^2$ in order to satisfy the condition $I_1(s-x(s)) \approx I_0(s)$, thus bringing I_1 in correspondence with I_0 in a best possible way. With the help of x and $I_1(s-x(s))$, one tries to understand, for instance, whether certain objects pictured in I_0 and I_1 are identical or if they have been subjected to intermittent alterations. Depending on the a priori available information about the shape of the pictured objects and their motion behaviour, very different approaches for the determination of the transformation x have been proposed in the literature. Assuming, for example, that only pixels with the same intensity should be mapped one to another, one arrives at the concept of the optical displacement or the optical flow, respectively.[03] Under different viewpoints, x has been determined as a flow governed by a Navier-Stokes equation (viscous fluid registration),[04] as a solution of a Monge-Kantorovič transportation problem,[05] as a rigid transformation in a higher-dimensional space[06] or by means of level-set methods.[07]

In many situations, it may be assumed with good reason that the changes in I_1 with respect to the reference image I_0 may be attributed to an *elastic deformation* of the pictured objects. This is particularly the case in the broad field of medical imaging since the behaviour of human tissue is governed by hyperelastic material laws.[08] For this reason, a large part of the literature is concerned with variational methods where x is sought as a linear-elastic[09] or hyperelastic deformation, respectively.[10] Moreover, a number of authors is performing the registration simultaneously with further tasks, e. g. segmentation.[11]

---

01) A detailed introduction may be found in [Modersitzki 04] and [Modersitzki 09]. Cf. also [Hintermüller/Keeling 09].

02) In the literature, the registration problem has been considered for image data on a domain $\Omega \subset \mathbb{R}^3$ as well (see, e. g. [Barbieri/Welk/Weickert 09] and [Pöschl/Modersitzki/Scherzer 09]). In the present paper, we confine ourselves to the two-dimensional case.

03) [Alvarez/Weickert/Sánchez 00], [Keeling/Ring 05]. Basic information about the concept of the optical flow may be found in [Aubert/Kornprobst 06], pp. 250 ff.

04) [Christensen/Rabbitt/Miller 96].

05) [Haker/Zhu/Tannenbaum/Angenent 04] and [Museyko/Stiglmayr/Klamroth/Leugering 09]; cf. also [Kaijser 98].

06) [Breitenreicher/Schnörr 09].

07) [Vemuri/Ye/Chen/Leonard 00].

08) See e. g. [Ogden 03]. Examples for polyconvex stored-energy functions applicable in this context may be found in [Balzani/Neff/Schröder/Holzapfel 06].

09) [Fischer/Modersitzki 03], [Haber/Modersitzki 04], [Henn/Witsch 00], [Henn/Witsch 01], [Modersitzki 04], pp. 77 ff.

10) [Droske/Rumpf 04], [Droske/Rumpf 07], [Le Guyader/Vese 09].

11) Cf. [Droske/Rumpf 07], [Le Guyader/Vese 09] as well as [Yezzi/Zollei/Kapur 01].

In the literature, the elastic registration problem has often been formulated as a multidimensional variational problem within Sobolev spaces. In these problems, the objective consists of a data fidelity term for minimization of the grey value difference $\big(I_1(s - x(s)) - I_0(s)\big)^2$ and a regularization term,[12] which will be chosen in such a way that the Euler-Lagrange equations of the problem describe a linear-elastic or hyperelastic deformation, respectively. In most cases, the numerical solution of the problems is effected with indirect methods.[13] In the present paper, this approach will be extended by incorporation of state constraints as well as restrictions for the partial derivatives of x into the variational problems.[14] On the one hand, such restrictions originate from additional information about the pictured objects (e. g. subregions, which remain unchanged or move in a rigid way); on the other hand, the validity of the underlying elasticity models is already bound by restrictions for the maximal shear stress generated by the deformation x.[15] Thus the given variational problems will be transformed into state-constrained *multidimensional control problems* of the so-called Dieudonné-Rashevsky type.[16] The numerical solution of these problems will be obtained by an efficient *direct method*.[17] In contrast to the indirect methods from the Calculus of Variations, the incorporation of additional state and control constraints produces no further difficulties within this direct approach.[18]

All approaches as yet mentioned are based on the assumption that there is an overall correlation between the greyscale intensity distributions as well as the geometrical properties of the template and reference image (unimodal registration). If a correspondence between the greyscale intensities of I_0 and I_1 cannot be expected from the outset, e. g. in the presence of data generated by different imaging devices or at different wave lenghts, one arrives at the problem of multimodal registration, which must exclusively be based on the geometrical information contained in the images.[19] In the present paper, however, we confine ourselves to *unimodal registration;* the application of optimal control methods to the multimodal registration problem will be reserved for a future publication.

The plan of the investigation is as follows: In *Section 2*, we explain the variational as well as the optimal control formulation of the elastic/hyperelastic image registration problem in more detail, adressing the relevance of additional state constraints and control restrictions. In both cases, the problems will be related to generical elasticity models. In order to justify the application of direct methods, we will then prove existence theorems for the multidimensional control problems. *Section 3* is devoted to the discretization of the problems and the methods for their numerical solution. In *Section 4*, we describe the visualization and evaluation of our results and document the test images used in the experiments. Finally, in *Section 5*, selected results of our numerical experiments will be presented and discussed.

---

[12] For regularization methods in image processing, cf. [Scherzer/Grasmair/Grossauer/Haltmeier/Lenzen 09], particularly pp. 53 ff., Sect. 3 and 4.

[13] See e. g. [Modersitzki 04], pp. 101 ff. On the contrary, [Modersitzki 09] is concerned with direct solution methods.

[14] Following the example of [Brune/Maurer/Wagner 09], [Franek/Franek/Maurer/Wagner 10], [Wagner 06], pp. 108 ff., [Wagner 08], pp. 26 ff., Sect. 4, and [Wagner 09], pp. 558 ff., Sect. 4 and 5.

[15] See, e. g. [Chmelka/Melan 76], pp. 38 – 45 (material sciences, linear-elastic model) as well as [Gasser/Holzapfel 02], p. 340 f., and the literature cited there (human tissue, different hyperelastic models).

[16] Cf. the introduction in [Wagner 09], pp. 543 – 545.

[17] Cf. again [Brune/Maurer/Wagner 09] and [Franek/Franek/Maurer/Wagner 10].

[18] The difficulties with the treatment of restrictions within indirect methods become apparent e. g. in [Haber/Modersitzki 04] and [Haber/Modersitzki 07a].

[19] [Droske/Rumpf 04], [Faugeras/Hermosillo 04], [Gallardo/Meju 03], [Haber/Modersitzki 07b], [Hermosillo/Chefd'hotel/Faugeras 02], [Liao/Yu/Bergsneider/Vese/Huang 03].

Notations.

Let $\Omega \subset \mathbb{R}^m$ be the closure of a bounded Lipschitz domain (in strong sense). Then $C^k(\Omega, \mathbb{R}^r)$ denotes the space of r-dimensional vector functions $f\colon \Omega \to \mathbb{R}^r$, whose components are continuous ($k = 0$) or k-times continuously differentiable ($k = 1, \ldots, \infty$), respectively; $L^p(\Omega, \mathbb{R}^r)$ denotes the space of r-dimensional vector functions $f\colon \Omega \to \mathbb{R}^r$, whose components are integrable in the pth power ($1 \leqslant p < \infty$) or are measurable and esentially bounded ($p = \infty$). $W_0^{1,p}(\Omega, \mathbb{R}^r)$ denotes the Sobolev space of r-dimensional vector functions $f\colon \Omega \to \mathbb{R}^r$ with compactly supported components, possessing first-order weak partial derivatives and belonging together with them to the space $L^p(\Omega, \mathbb{R})$ ($1 \leqslant p < \infty$). $W_0^{1,\infty}(\Omega, \mathbb{R}^r)$ is understood as the Sobolev space of all r-vector functions $f\colon \Omega \to \mathbb{R}^r$ with Lipschitz continuous components and boundary values zero. [20] Jx denotes the Jacobi matrix of the vector function $x \in W_0^{1,p}(\Omega, \mathbb{R}^r)$. The symbol $\mathfrak{o}$ denotes, depending on the context, the zero element or the zero function of the underlying space. Finally, the abbreviation "$(\forall)\, s \in \mathrm{A}$" has to be read as "for almost all $s \in \mathrm{A}$" or "for all $s \in \mathrm{A}$ except a Lebesgue null set".

2. Elastic/hyperelastic image registration as a multidimensional control problem.

a) The variational approach.

As mentioned in the introduction, in the present paper we will consider *generical* elasticity models rather than concrete ones. An image registration problem within Sobolev space, which is based on a linear-elastic model, may be stated as follows: [21]

$$(\mathrm{V})_{lin}\colon \quad F(x) = \int_\Omega \Big(I_1(\,s - x(s)\,) - I_0(s) \Big)^2 \, ds \;+\; \mu \cdot \int_\Omega \sum_{i,j=1}^{2} \Big(\frac{\partial x_i(s)}{\partial s_j} \;+\; \frac{\partial x_j(s)}{\partial s_i} \Big)^2 \, ds \;\longrightarrow\; \inf\!\,! \,; \tag{2.1}$$

$$x \in W_0^{1,p}(\Omega, \mathbb{R}^2) \tag{2.2}$$

with measurable, bounded image data $I_0(s)$, $I_1(s)\colon \Omega \to [\,0\,,\,1\,]$, [22] $2 \leqslant p < \infty$ and a regularization parameter $\mu > 0$.
If the deformations of the imaged objects, instead, are supposed to obey a generic hyperelastic material law, one arrives at the problem [23]

$$(\mathrm{V})_{hyp}\colon \quad F(x) = \int_\Omega \Big(I_1(\,s - x(s)\,) - I_0(s) \Big)^2 \, ds \;+\; \mu \cdot \int_\Omega \Big(c_1 \, \big\| \, E_2 - Jx(s) \, \big\|^{\,p} + c_2 \, \big(\mathrm{Det}\,(\,E_2 - Jx(s)\,) \big)^2 \Big) \, ds \;\longrightarrow\; \inf\!\,! \,; \tag{2.3}$$

$$x \in W_0^{1,p}(\Omega, \mathbb{R}^2) \tag{2.4}$$

with image data I_0, I_1 as above, $2 \leqslant p < \infty$, $\mu > 0$ and positive weights $c_1, c_2 > 0$. E_2 denotes the $(2,2)$-unit matrix. As matrix norm, we use $\| \, M \, \| = \mathrm{trace}\,(\,M^{\mathrm{T}} M\,)$. While the linear-elastic image registration leads

---

[20] Cf. [Evans/Gariepy 92], p. 131, Theorem 5.

[21] We refer to [Henn/Witsch 01], p. 1079 f.

[22] Note that the integral functionals (2.1) and (2.3) are well-defined for $s - x(s) \in \Omega$ $(\forall)\, s \in \Omega$ only. This condition, however, can be eliminated if the image data I_0 and I_1 are embedded into a sufficiently wide black frame, i. e. they will be extended by zero to $\mathbb{R}^2 \setminus \Omega$; cf. [Henn/Witsch 01], p. 1078.

[23] [Droske/Rumpf 04], p. 673 f.

to a convex problem, the objective within the hyperelastic image registration problem involves a polyconvex regularization term. [24)]

b) Approximation of the fidelity term.

In the practical dealing with the problems $(\mathrm{V})_{lin}$ and $(\mathrm{V})_{hyp}$ the direct evaluation of the composite function $I_1(\,s - x(s)\,)$ effects a substantial difficulty. Assuming first that the given image data I_1 are sufficiently smooth, we use a second-order Taylor expansion [25)]

$$I_1(\,s-x(s)\,) \;=\; I_1(s) \;-\; \nabla\, I_1(s)^{\mathrm{T}}\, x(s) \;+\; \tfrac{1}{2}\, x(s)^{\mathrm{T}}\, \nabla^2 I_1(s)\, x(s) \;+\; R(\,x(s), y(s)\,) \tag{2.5}$$

with the third-order remainder term $R(\,x(s), y(s)\,) \;=\; \frac{1}{6}\, y(s) \cdot \|\, x(s)\,\|^3$. Since in most cases, the assumption $I_1 \in C^3(\Omega, \mathbb{R})$ is unrealistic, the derivatives of I_1 will be replaced by further approximations $\nabla I_1 \approx DI_1 \in L^\infty(\Omega, \mathbb{R}^2)$ and $\nabla^2 I_1 \;\approx\; D^2 I_1 \;\in\; L^\infty(\Omega, \mathbb{R}^{2\times 2})$ based on smoothing and forming of finite differences (see $(3.7) - (3.11)$ below). Thus the integrand within the fidelity term will be finally approximated by

$$I_1(\,s-x(s)\,) - I_0(s) \;\approx\; I_1(s) \;-\; DI_1(s)^{\mathrm{T}}\, x(s) \;+\; \tfrac{1}{2}\, x(s)^{\mathrm{T}}\, D^2 I_1(s)\, x(s) \;+\; \tfrac{1}{6}\, y(s) \cdot \|\, x(s)\,\|^3 \;-\; I_0(s)\,. \tag{2.6}$$

When inserting — motivated by the addition of uniform gradient constraints to $(\mathrm{V})_{lin}$ and $(\mathrm{V})_{hyp}$ below — functions $x \in W_0^{1,\infty}(\Omega, \mathbb{R}^2)$ into (2.6), we may identify $y(\,\cdot\,)$ as a L^∞ function. The character of x as an elastic deformation will be preserved as long as y remains sufficiently small, which will be ensured by an additional state constraint $|\, y(s)\,| \leqslant \eta_{max}$.

c) Incorporation of constraints.

1) Constraints for the admissible shear stresses. On the one hand, these constraints are mandatory in order to ensure the validity of the underlying elasticity models. [26)] Independently, on the other hand, the introduction of such constraints may be motivated by the necessity of an additional regularization of the problems. This is particularly true if — after concretization of the material law — the former regularization parameter μ must be fixed as a material constant. The modulus of the shear stress generated by the deformation x is proportional to $\|\, Jx(s)\,\|$, consequently, we arrive at a convex gradient constraint

$$Jx(s) \;\in\; \mathrm{K} \;\subset\; \mathbb{R}^{2\times 2} \quad (\forall)\, s \in \Omega \tag{2.7}$$

where $\mathrm{K} \subset \mathbb{R}^{2\times 2}$ is a convex norm body with $\mathfrak{o} \in \mathrm{int}\,(\mathrm{K})$.

2) Landmarks. The correspondences

$$I_1\big(\,s_k - x(s_k)\,\big) \;=\; I_0(\tilde{s}_k) \quad\Longleftrightarrow\quad x(s_k) \;=\; \begin{pmatrix} c_{1,k} \\ c_{2,k} \end{pmatrix} \;=\; \begin{pmatrix} s_{k,1} - \tilde{s}_{k,1} \\ s_{k,2} - \tilde{s}_{k,2} \end{pmatrix},\;\; 1 \leqslant k \leqslant K\,, \tag{2.8}$$

determine exactly the values of the deformation x in the points $s_1, \,\ldots\, , s_K \in \Omega$.

3) Nearly undistorted subregions. The situation where the deformation x leaves a subregion $\Theta \subset \Omega$ nearly undistorted will be described by a state constraint

$$\|\, x(s)\,\| \;\leqslant\; \varepsilon \quad \forall\, s \in \Theta \tag{2.9}$$

[24)] Cf. [Ball 77] and [Dacorogna 08], pp. 156 ff.

[25)] A *first-order* Taylor expansion leads back to the determination of the optical flow.

[26)] See Footnote 15 above.

with sufficiently small $\varepsilon > 0$ (if $\varepsilon = 0$ then Θ will be not affected at all).

4) Subregions subjected to a pure translation. In this case, on the subregion $\Theta \subseteq \Omega$ we have $s - x(s) = s - s_0$ and $Jx(s) = \mathfrak{o}$. Consequently, we will introduce

$$\| Jx(s) \| \leqslant \varepsilon \quad (\forall)\, s \in \Theta \tag{2.10}$$

with sufficiently small $\varepsilon > 0$ as an additional gradient constraint.

The introduction of *polyconvex* gradient constraints, which enforce a *rigid deformation* or a *bijective deformation of a subregion*, will be investigated in [WAGNER 10].

d) Reformulation of the problems within the framework of multidimensional control.

To $(\mathrm{V})_{lin}$ and $(\mathrm{V})_{hyp}$, we add the convex gradient restriction (2.7) thus converting both problems into multidimensional control problems of Dieudonné-Rashevsky type. Further, we replace the term $I_1(s - x(s))$ within the objectives by its approximation (2.6). According to the discussion in Subsection 2.b), y will be specified as a measurable function, which is uniformly bounded by η_{max}. As a result, we obtain the following state-constrained optimal control problems:

$$(\mathrm{P})_{lin}\colon \quad F(x,y) = \int_\Omega \Big(I_1(s) - DI_1(s)^{\mathrm{T}}\, x(s) + \tfrac{1}{2}\, x(s)^{\mathrm{T}}\, D^2 I_1(s)\, x(s) + \tfrac{1}{6}\, y(s)\, \| x(s) \|^3 - I_0(s) \Big)^2 ds$$
$$+ \mu \cdot \int_\Omega \sum_{i,j=1}^{2} \Big(\frac{\partial x_i(s)}{\partial s_j} + \frac{\partial x_j(s)}{\partial s_i} \Big)^2 ds \longrightarrow \inf\,! \,; \tag{2.11}$$
$$(x,y) \in W_0^{1,p}(\Omega, \mathbb{R}^2) \times L^\infty(\Omega, \mathbb{R})\,; \tag{2.12}$$
$$|\, y(s) \,| \leqslant \eta_{max} \ (\forall)\, s \in \Omega\,; \tag{2.13}$$
$$Jx(s) \in \mathrm{K} \ (\forall)\, s \in \Omega \tag{2.14}$$

(linear-elastic image registration) and

$$(\mathrm{P})_{hyp}\colon \quad F(x,y) = \int_\Omega \Big(I_1(s) - DI_1(s)^{\mathrm{T}}\, x(s) + \tfrac{1}{2}\, x(s)^{\mathrm{T}}\, D^2 I_1(s)\, x(s) + \tfrac{1}{6}\, y(s)\, \| x(s) \|^3 - I_0(s) \Big)^2 ds$$
$$+ \mu \cdot \int_\Omega \Big(c_1 \, \big\| E_2 - Jx(s) \big\|^{\,p} + c_2 \, \big(\mathrm{Det}\, (\, E_2 - Jx(s)\,) \big)^2 \Big)\, ds \longrightarrow \inf\,! \,; \tag{2.15}$$
$$(x,y) \in W_0^{1,p}(\Omega, \mathbb{R}^2) \times L^\infty(\Omega, \mathbb{R})\,; \tag{2.16}$$
$$|\, y(s) \,| \leqslant \eta_{max} \ (\forall)\, s \in \Omega\,; \tag{2.17}$$
$$Jx(s) \in \mathrm{K} \ (\forall)\, s \in \Omega \tag{2.18}$$

(hyperelastic image registration) with measurable, bounded data I_0, $I_1 \in L^\infty(\Omega, \mathbb{R})$, $DI_1 \in L^\infty(\Omega, \mathbb{R}^2)$ and $D^2 I_1 \in L^\infty(\Omega, \mathbb{R}^{2\times 2})$, $1 \leqslant p < \infty$, an uniform bound $\eta_{max} > 0$ for the fitting variable in the remainder in the Taylor expansion, a regularization parameter $\mu > 0$ and positive weights c_1, $c_2 > 0$. $\mathrm{K} \subset \mathbb{R}^{2\times 2}$ is a convex body with $\mathfrak{o} \in \mathrm{int}\,(\mathrm{K})$. Further state constraints and control restrictions of the shape $(2.8) - (2.10)$ may be easily included. As a consequence of the control restrictions (2.14) and (2.18), all feasible pairs (x, y) in $(\mathrm{P})_{lin}$ and $(\mathrm{P})_{hyp}$ belong to the space $W_0^{1,\infty}(\Omega, \mathbb{R}^2) \times L^\infty(\Omega, \mathbb{R})$ independent of the choice of the exponent $1 \leqslant p < \infty$.

Remarks. 1) Note that certain *rigid motions* are contained within the feasible domains of $(\mathrm{P})_{lin}$ as well as of $(\mathrm{P})_{hyp}$. Since $\mathrm{K} \subset \mathbb{R}^{2\times 2}$ contains a four-dimensional cube $[\, R\,,\, R\,]^4$ in a neighborhood of the origin,

all rotations satisfying $Jx(s) = E_2 - \left(\begin{smallmatrix}\cos\alpha & -\sin\alpha \\ \sin\alpha & \cos\alpha\end{smallmatrix}\right)$ with $|\,\alpha\,| \leqslant \arcsin(R)$ and $|\,\alpha\,| \leqslant \arccos(1-R)$ as well as arbitrary translations on given subregions $\Theta \subseteq \Omega$ are feasible.

2) In the numerical experiments in Sections $3-5$, the convex body in the control restrictions will be immediately $\mathrm{K} = [\,-R\,,\,R\,]^4$ where $R > 0$ is considered as an additional parameter.

e) Existence of global minimizers.

In order to justify the application of direct methods to the numerical solution of the optimal control problems $(\mathrm{P})_{lin}$ and $(\mathrm{P})_{hyp}$, we must first ensure the existence of global minimizers. In our proofs, we refer to theorems from [Dacorogna 08] and [Wagner 08].

Theorem 2.1. (Existence theorem for $(\mathrm{P})_{lin}$) [27] *1) Let the problem $(\mathrm{P})_{lin}$ be given with all assumptions about the data mentioned above. Then the problem admits a global minimizer $(\hat{x},\hat{y}) \in W_0^{1,\infty}(\Omega,\mathbb{R}^2) \times L^\infty(\Omega,\mathbb{R})$.*

2) Assertion 1) remains true if $(\mathrm{P})_{lin}$ is augmented with additional state constraints of the shape (2.8), (2.9) or control constraints of the shape (2.10) where $\Theta \subset \Omega$, $\mathrm{int}\,(\Theta) \neq \emptyset$, is a compact subset of Ω.

Proof. 1) • *Step 1: The problem $(\mathrm{P})_{lin}$ admits a minimizing sequence with a feasible limit element.* Since $F(x,y) \geqslant 0$ and the zero solution is feasible, problem $(\mathrm{P})_{lin}$ admits a minimizing sequence $\{\,(x^N,y^N)\,\}$. It follows from (2.13) and (2.14) that $\|\,x^N\,\|_{W_0^{1,\infty}(\Omega,\mathbb{R}^2)}$ as well as $\|\,y^N\,\|_{L^\infty(\Omega,\mathbb{R})}$ remain bounded. Consequently, after a passage to appropriate subsequences we may assume that the minimizing sequence possesses a limit element $(\hat{x},\hat{y}) \in W_0^{1,\infty}(\Omega,\mathbb{R}^2) \times L^\infty(\Omega,\mathbb{R})$ with

$$x^N \to^{C^0(\Omega,\mathbb{R}^2)} \hat{x}\,,\quad Jx^N \overset{*}{\rightharpoonup}^{L^\infty(\Omega,\mathbb{R}^4)} J\hat{x} \quad\text{and}\quad y^N \overset{*}{\rightharpoonup}^{L^\infty(\Omega,\mathbb{R})} \hat{y}\,. \tag{2.19}$$

Under the weak*-convergence of $\{\,y^N\,\}$ and $\{\,Jx^N\,\}$, the convex state constraint (2.13) as well as the convex gradient constraint (2.14) will be conserved, and $(\hat{x},\hat{y})$ is feasible in $(\mathrm{P})_{lin}$.

• *Step 2: Decomposition of the objective.* Denote by $\xi \in \mathbb{R}^2$, $\eta \in \mathbb{R}$ and $v \in \mathbb{R}^{2\times 2}$ the placeholders for x, y and Jx. Further, let $\varrho_{\mathrm{K}}(\,\cdot\,)$ denote the indicator function of the convex body K. Then the integrand within the objective admits the following decomposition:

$$f(s,\xi,\eta,v) \;=\; \Big(\, f_0(s,\xi) \,+\, \mu \cdot \sum_{i,j=1}^{2} \big(\, v_{ij} + v_{ji} \,\big)^2 \,+\, \varrho_{\mathrm{K}}(v) \,\Big) \,+\, \Big(\, \eta \cdot f_1(s,\xi) \,+\, \eta^2 \cdot f_2(s,\xi) \,\Big) \quad\text{with} \tag{2.20}$$

$$f_0(s,\xi) \;=\; \big(\, I_1(s) - DI_1(s)^{\mathrm{T}}\,\xi + \tfrac{1}{2}\,\xi^{\mathrm{T}}\,D^2I_1(s)\,\xi - I_0(s) \,\big)^2\,; \tag{2.21}$$

$$f_1(s,\xi) \;=\; \tfrac{1}{3}\,|\,\xi\,|^3\,\big(\, I_1(s) - DI_1(s)^{\mathrm{T}}\,\xi + \tfrac{1}{2}\,\xi^{\mathrm{T}}\,D^2I_1(s)\,\xi - I_0(s) \,\big)\,; \tag{2.22}$$

$$f_2(s,\xi) \;=\; \tfrac{1}{36}\,|\,\xi\,|^6\,. \tag{2.23}$$

• *Step 3: Application of lower semicontinuity theorems.* Due to the essential boundedness of I_0, I_1, DI_1 and D^2I_1, the first member in (2.20) obeys the growth condition [28]

$$\begin{aligned}
&\big|\, f_0(s,\xi) \,+\, \mu \cdot \sum_{i,j=1}^{2} \big(\, v_{ij} + v_{ji} \,\big)^2 \,+\, \varrho_{\mathrm{K}}(v) \,\big| \\
&\quad\leqslant \Big(\, \big|\, I_1(s) - I_0(s) \,\big| \,+\, \big|\, DI_1(s) \,\big| \cdot \big|\, \xi \,\big| + \tfrac{1}{2}\,\big\|\, D^2I_1(s) \,\big\| \cdot \big|\, \xi \,\big|^2 \,\Big)^2 \,+\, \mu \cdot \sum_{i,j=1}^{2} \big(\, v_{ij} + v_{ji} \,\big)^2 \qquad (2.24) \\
&\quad\leqslant \Big(\, 2 + C_1\,\big|\, \xi \,\big| + \tfrac{1}{2}\,C_2\,\big|\, \xi \,\big|^2 \,\Big)^2 \,+\, \mu \cdot \sum_{i,j=1}^{2} \big(\, v_{ij} + v_{ji} \,\big)^2 \quad (\forall)\, s \in \Omega \;\; \forall\,(\xi,v) \in \mathbb{R}^2 \times \mathrm{K}\,, \qquad (2.25)
\end{aligned}$$

[27] Cf. [Wagner 08], p. 27, Theorem 4.1., 1).

[28] Cf. [Wagner 08], p. 27, (4.10) – (4.11).

consequently, we may apply [WAGNER 08], p. 4, Theorem 1.4., to the expression, and its convexity with respect to v implies the lower semicontinuity relation

$$\int_\Omega \Big(f_0(s,\hat{x}(s)) \,+\, \mu \cdot \sum_{i,j=1}^{2} \Big(\frac{\partial \hat{x}_i}{\partial s_j}(s) + \frac{\partial \hat{x}_j}{\partial s_i}(s) \Big)^2 \Big)\, ds$$
$$\leqslant \liminf_{N\to\infty} \int_\Omega \Big(f_0(s,x^N(s)) \,+\, \mu \cdot \sum_{i,j=1}^{2} \Big(\frac{\partial x_i^N}{\partial s_j}(s) + \frac{\partial x_j^N}{\partial s_i}(s) \Big)^2 \Big)\, ds\,. \tag{2.26}$$

From $f_2(s,\xi) \geqslant 0$, we obtain after inserting of $\xi = \hat{x}(s)$ the following estimate for the second member:

$$\eta \cdot f_1(s,\hat{x}(s)) \,+\, \eta^2 \cdot f_2(s,\hat{x}(s)) \,\geqslant\, \eta \cdot f_1(s,\hat{x}(s)) \quad (\forall)\, s \in \Omega \;\forall (\xi,\eta,v) \in \mathbb{R}^2 \,\times\, \mathbb{R} \,\times \mathbb{R}^{2\times 2}\,, \tag{2.27}$$

where $f_1(\,\cdot\,,\hat{x}(\,\cdot\,)) \in L^1(\Omega,\mathbb{R})$. Consequently, [DACOROGNA 08], p. 96, Theorem 3.23., together with p. 97, Remark 3.25., (ii), may be applied:

$$\int_\Omega \Big(\hat{y}(s)\, f_1(s,\hat{x}(s)) \,+\, \hat{y}(s)^2\, f_2(s,\hat{x}(s)) \Big)\, ds \,\leqslant\, \liminf_{N\to\infty} \int_\Omega \Big(y^N(s)\, f_1(s,\hat{x}(s)) \,+\, y^N(s)^2\, f_2(s,\hat{x}(s)) \Big)\, ds\,. \tag{2.28}$$

From the uniform convergence of $\{\, x^N \,\}$ and the essential boundedness of $\{\, y^N \,\}$, it follows that

$$\liminf_{N\to\infty} \Big| \int_\Omega \Big(y^N(s)\, f_1(s,x^N(s)) \,+\, y^N(s)^2\, f_2(s,x^N(s)) \,-\, y^N(s)\, f_1(s,\hat{x}(s)) \,-\, y^N(s)^2\, f_2(s,\hat{x}(s)) \Big)\, ds \Big|$$
$$\leqslant \liminf_{N\to\infty} \int_\Omega \Big(\big|\, f_1(s,x^N(s)) - f_1(s,\hat{x}(s)) \,\big| \cdot \eta_{max} \,+\, \big|\, f_2(s,x^N(s)) - f_2(s,\hat{x}(s)) \,\big| \cdot \eta_{max}^2 \Big)\, ds \,=\, 0\,. \tag{2.29}$$

• *Step 4: Conclusion.* Denoting the minimal value of $(\mathrm{P})_{lin}$ by m, we obtain from (2.26), (2.28) and (2.29):

$$m \,\leqslant\, F(\hat{x},\hat{y}) \,\leqslant\, \liminf_{N\to\infty} \int_\Omega \Big(f_0(s,x^N(s)) \,+\, \mu \cdot \sum_{i,j=1}^{2} \Big(\frac{\partial x_i^N}{\partial s_j}(s) + \frac{\partial x_j^N}{\partial s_i}(s) \Big)^2 \Big)\, ds \tag{2.30}$$
$$+\, \liminf_{N\to\infty} \int_\Omega \Big(y^N(s)\, f_1(s,\hat{x}(s)) \,+\, y^N(s)^2\, f_2(s,\hat{x}(s)) \Big)\, ds$$
$$+\, \liminf_{N\to\infty} \int_\Omega \Big(y^N(s)\, f_1(s,x^N(s)) \,+\, y^N(s)^2\, f_2(s,x^N(s)) \,-\, y^N(s)\, f_1(s,\hat{x}(s)) \,-\, y^N(s)^2\, f_2(s,\hat{x}(s)) \Big)\, ds$$
$$\leqslant \liminf_{N\to\infty} F(x^N,y^N) \,=\, \lim_{N\to\infty} F(x^N,y^N) \,=\, m\,,$$

and $(\hat{x},\hat{y})$ is a global minimizer of $(\mathrm{P})_{lin}$.

2) After addition of further state constraints (2.8), (2.9) or control restrictions (2.10) to $(\mathrm{P})_{lin}$, the zero solution remains feasible. Consequently, for the new problem there exists a minimizing sequence $\{\, (x^N,y^N) \,\}$ with $x^N \to^{C^0(\Omega,\mathbb{R}^2)} \hat{x}$, $Jx^N \overset{*}{\rightharpoonup}^{L^\infty(\Omega,\mathbb{R}^4)} J\hat{x}$ and $y^N \rightharpoonup^{L^\infty(\Omega,\mathbb{R})} \hat{y}$ as well, for which all conclusions from Part 1) remain valid. We have only to check whether its limit element obeys the additional constraints. For (2.8) and (2.9), this holds as a consequence of the uniform convergence of $\{\, x^N \,\}$ and the continuity of the norm in $\mathbb{R}^2$; for (2.10), we observe that the weak*-convergence of $\{\, Jx^N \,\}$ im $L^\infty(\Omega,\mathbb{R}^4)$ implies the weak*-convergence of the restrictions $\{\, Jx^N \,|\, \Theta \,\}$ in $L^\infty(\Theta,\mathbb{R}^4)$. However, the convex constraint (2.10) on Θ will be conserved under the passage to the weak*-limit element. ∎

Theorem 2.2. (Existence theorem for $(\mathrm{P})_{hyp}$ **)** [29] *1) Under the assumptions about the data mentioned above, the problem* $(\mathrm{P})_{hyp}$ *admits a global minimizer* $(\hat{x},\hat{y}) \in W_0^{1,\infty}(\Omega,\mathbb{R}^2) \,\times\, L^\infty(\Omega,\mathbb{R})$ *as well.*

[29] Cf. [WAGNER 08], p. 29, Theorem 4.2., 1).

2) Assertion 1) remains true if $(\mathrm{P})_{hyp}$ *is augmented with additional state constraints of the shape* (2.8), (2.9) *or control constraints of the shape* (2.10) *where* $\Theta \subset \Omega$, $\mathrm{int}\,(\Theta) \neq \emptyset$, *is a compact subset of* Ω.

Proof. 1) Reasoning as in the proof of Theorem 2.1., 1), we represent the integrand as (2.31)

$$f(s,\xi,\eta,v) \;=\; \Big(f_0(s,\xi) + \mu \cdot \Big(c_1 \,\big\|\, E_2 - v \,\big\|^p + c_2 \,\big(\,\mathrm{Det}\,(E_2 - v)\,\big)^2 \Big) + \varrho_{\mathrm{K}}(v) \Big) + \Big(\eta \cdot f_1(s,\xi) + \eta^2 \cdot f_2(s,\xi) \Big)$$

with f_0, f_1 and f_2 according to (2.21) – (2.23). The first member is polyconvex with respect to $v \in \mathbb{R}^{2\times 2}$ and satisfies the growth condition [30)]

$$\begin{aligned} &\Big| f_0(s,\xi) \,+\, \mu \cdot \Big(c_1 \,\big\|\, E_2 - v \,\big\|^p \,+\, c_2 \,\big(\,\mathrm{Det}\,(E_2 - v)\,\big)^2 \Big) \,+\, \varrho_{\mathrm{K}}(v) \,\Big| \qquad (2.32)\\ &\leqslant \Big(\big|\, I_1(s) - I_0(s) \,\big| \,+\, \big|\, DI_1(s) \,\big| \cdot |\,\xi\,| + \tfrac{1}{2} \,\big\|\, D^2 I_1(s) \,\big\| \cdot |\,\xi\,|^2 \Big)^2 + \mu \cdot \Big(c_1 \,\big\|\, E_2 - v \,\big\|^p \,+\, c_2 \,\big(\,\mathrm{Det}\,(E_2 - v)\,\big)^2 \Big)\\ &\leqslant \Big(2 + C_1\,|\,\xi\,| + \tfrac{1}{2}\,C_2\,|\,\xi\,|^2 \Big)^2 \,+\, \mu \cdot \Big(c_1 \,\big\|\, E_2 - v \,\big\|^p \,+\, c_2 \,\big(\,\mathrm{Det}\,(E_2 - v)\,\big)^2 \Big) \quad (\forall)\, s \in \Omega \;\; \forall\, (\xi, v) \in \mathbb{R}^2 \times \mathrm{K}\,, \end{aligned}$$

consequently, [Wagner 08], p. 4, Theorem 1.4., implies the lower semicontinuity relation

$$\begin{aligned} &\int_\Omega \Big(f_0(s,\hat{x}(s)) \,+\, \mu \cdot \Big(c_1 \,\big\|\, E_2 - J\hat{x}(s) \,\big\|^p \,+\, c_2 \,\big(\,\mathrm{Det}\,(\,E_2 - J\hat{x}(s)\,)\,\big)^2 \Big) \Big)\, ds\\ &\leqslant \liminf_{N\to\infty} \int_\Omega \Big(f_0(s,x^N(s)) \,+\, \mu \cdot \Big(c_1 \,\big\|\, E_2 - Jx^N(s) \,\big\|^p \,+\, c_2 \,\big(\,\mathrm{Det}\,(\,E_2 - Jx^N(s)\,)\,\big)^2 \Big) \Big)\, ds\,. \qquad (2.33) \end{aligned}$$

Then the existence of a global minimizer may be ensured as in Theorem 2.1., 1).

2) This assertion may be proven in complete analogy to Theorem 2.1., 2). ∎

3. Numerical solution by direct methods.

For the numerical solution of the multidimensional control problems $(\mathrm{P})_{lin}$ and $(\mathrm{P})_{hyp}$, we adopt the principle "first discretize, then optimize". In all problems, we will work with the control restriction $Jx(s) \in \mathrm{K} = [\,-R\,,\,R\,]^4$. Within the square domain $\Omega = [\,0\,,\,K\,] \times [\,0\,,\,L\,]$ with $K = L = 2^N$, we generate a regular triangulation, [31)] introducing first a grid of squares $\mathrm{Q}_{k,l}$ with edge length 1 and then splitting every square along the principal diagonal into two triangles $\Delta'_{k,l} = \Delta(s_{k-1,l-1}, s_{k,l-1}, s_{k,l})$ and $\Delta''_{k,l} = \Delta(s_{k-1,l-1}, s_{k,l}, s_{k-1,l})$. With $f(s,\xi,\eta,v)$ as abbreviation for the integrand within the objective, the discretized problem may be stated as follows: [32)]

$$\begin{aligned} (\mathrm{D})_N: \quad &\widetilde{F}\big(\,\xi^{(1)}_{0,0},\,\ldots\,,\,\xi^{(2)}_{K,L},\,\eta_{0,0},\,\ldots\,,\,\eta_{K,L},\,v^{(1,1)}_{1,1},\,\ldots\,,\,v^{(2,4)}_{K,L}\,\big) \;=\; \frac{1}{2}\cdot\sum_{k=1}^{K}\sum_{l=1}^{L}\Big(f\big(\,s_{k-1,l-1},\begin{pmatrix}\xi^{(1)}_{k-1,l-1}\\ \xi^{(2)}_{k-1,l-1}\end{pmatrix},\\ &\eta_{k-1,l-1}\,,\begin{pmatrix} v^{(1,1)}_{k,l} & v^{(1,2)}_{k,l}\\ v^{(2,1)}_{k,l} & v^{(2,2)}_{k,l}\end{pmatrix}\big) + f\big(\,s_{k,l},\begin{pmatrix}\xi^{(1)}_{k,l}\\ \xi^{(2)}_{k,l}\end{pmatrix},\eta_{k,l}\,,\begin{pmatrix} v^{(1,3)}_{k,l} & v^{(1,4)}_{k,l}\\ v^{(2,3)}_{k,l} & v^{(2,4)}_{k,l}\end{pmatrix}\big)\Big) \;\longrightarrow\; \inf!\,; \qquad (3.1)\\ &\big(\,\xi^{(1)}_{0,0},\,\ldots,\,\xi^{(2)}_{K,L},\,\eta_{0,0},\,\ldots\,,\,\eta_{K,L},\,v^{(1,1)}_{1,1},\,\ldots,\,v^{(2,4)}_{K,L}\,\big) \;\in\; \mathbb{R}^{3(K+1)(L+1)} \times \mathbb{R}^{8KL}\,; \qquad (3.2) \end{aligned}$$

[30)] Cf. [Wagner 08], p. 29, (4.17) – (4.18).

[31)] Cf. [Goering/Roos/Tobiska 93], pp. 28 and 40, (Z1) – (Z4), and p. 138, (Z5).

[32)] Cf. [Franek/Franek/Maurer/Wagner 10], p. 3 f., (2.7) – (2.14).

$$\xi_{0,l}^{(i)} = \xi_{K,l}^{(i)} = 0\,,\ \xi_{k,0}^{(i)} = \xi_{k,L}^{(i)} = 0\,,\quad i = 1,\,2\,,\ 0 \leqslant k \leqslant K\,,\ 0 \leqslant l \leqslant L\,; \tag{3.3}$$

$$\begin{pmatrix} v_{k,l}^{(i,1)} & v_{k,l}^{(i,2)} \\ v_{k,l}^{(i,3)} & v_{k,l}^{(i,4)} \end{pmatrix} = \begin{pmatrix} \xi_{k,l-1}^{(i)} - \xi_{k-1,l-1}^{(i)} & \xi_{k,l}^{(i)} - \xi_{k,l-1}^{(i)} \\ \xi_{k,l}^{(i)} - \xi_{k-1,l}^{(i)} & \xi_{k-1,l}^{(i)} - \xi_{k-1,l-1}^{(i)} \end{pmatrix},\ i = 1,\,2\,,\ 1 \leqslant k \leqslant K\,,\ 1 \leqslant l \leqslant L\,; \tag{3.4}$$

$$\left|\,\eta_{k,l}\,\right| \leqslant \eta_{max}\,,\quad 0 \leqslant k \leqslant K\,,\ 0 \leqslant l \leqslant L\,; \tag{3.5}$$

$$\left|\,v_{k,l}^{(i,1)}\,\right| \leqslant R\,,\ \left|\,v_{k,l}^{(i,2)}\,\right| \leqslant R\,,\ \left|\,v_{k,l}^{(i,3)}\,\right| \leqslant R\,,\ \left|\,v_{k,l}^{(i,4)}\,\right| \leqslant R\,,\ i = 1,\,2\,,\ 1 \leqslant k \leqslant K\,,\ 1 \leqslant l \leqslant L\,; \tag{3.6}$$

The partial derivatives of I_1 have been approximated in $\mathrm{Q}_{k,l}$ as follows:

$$\frac{\partial I_1}{\partial s_1}(s) \approx D_{s_1} I_1(s) = \frac{1}{9} \cdot \sum_{i,j=-1}^{1} \Big(\frac{1}{2} \big(I_1(s_{k+1+i\,,\,l+j}) - I_1(s_{k-1+i\,,\,l+j}) \big) \Big)\,; \tag{3.7}$$

$$\frac{\partial I_1}{\partial s_2}(s) \approx D_{s_2} I_1(s) = \frac{1}{9} \cdot \sum_{i,j=-1}^{1} \Big(\frac{1}{2} \big(I_1(s_{k+i\,,\,l+1+j}) - I_1(s_{k+i\,,\,l-1+j}) \big) \Big)\,; \tag{3.8}$$

$$\frac{\partial^2 I_1}{(\partial s_1)^2}(s) \approx D_{s_1 s_1}^2 I_1(s) = \frac{1}{9} \cdot \sum_{i,j=-1}^{1} \Big(\frac{1}{2} \big(I_1(s_{k+1+i\,,\,l+j}) - 2\, I_1(s_{k+i\,,\,l+j}) + I_1(s_{k-1+i\,,\,l+j}) \big) \Big)\,; \tag{3.9}$$

$$\frac{\partial^2 I_1}{\partial s_1\, \partial s_2}(s) \approx D_{s_1 s_2}^2 I_1(s) = \frac{1}{9} \cdot \sum_{i,j=-1}^{1} \Big(\frac{1}{4} \big(I_1(s_{k+1+i\,,\,l+1+j}) - I_1(s_{k-1+i\,,\,l+1+j}) \tag{3.10}$$

$$- I_1(s_{k+1+i\,,\,l-1+j}) + I_1(s_{k-1+i\,,\,l-1+j}) \big) \Big)\,;$$

$$\frac{\partial^2 I_1}{(\partial s_2)^2}(s) \approx D_{s_2 s_2}^2 I_1(s) = \frac{1}{9} \cdot \sum_{i,j=-1}^{1} \Big(\frac{1}{2} \big(I_1(s_{k+i\,,\,l+1+j}) - 2\, I_1(s_{k+i\,,\,l+j}) + I_1(s_{k+i\,,\,l-1+j}) \big) \Big)\,. \tag{3.11}$$

The evaluation of the necessary optimality conditions (Karush-Kuhn-Tucker conditions) for $(\mathrm{D})_N$ results in large systems of nonlinear equations, which may be solved with high precision and efficiency by interior-point methods. [33] We used MATLAB as the input/output platform for the image data; the discretized problem has been formulated with the help of the modelling language AMPL [34] and then transferred to the interior-point solver IPOPT. [35] The results have been represented and evaluated with MATLAB again.

The convergence of the discretization method with respect to the x-component of the solutions can be ensured in analogy to [Franek/Franek/Maurer/Wagner 10], p. 10, Corollary 2.7., assuming that the image data I_1 are sufficiently smooth. [36] We dispensed, however, in the present paper completely with assumptions allowing the proof of an analogous error estimate for $\| y - \hat{y} \|_{L^\infty(\Omega,\mathbb{R})}$. [37]

[33] See, for example, [Jansen 97].

[34] [Fourer/Gay/Kernighan 03].

[35] [Laird/Wächter 09], [Wächter/Biegler 06]. The experiments have been performed with version 3.6.1., compiled with the MA27 routine.

[36] The assumptions [Franek/Franek/Maurer/Wagner 10], p. 5, (2.19) and (2.20), will be satisfied e. g. for $I_1 \in C_0^2(\Omega,\mathbb{R}) \cap C^3(\Omega,\mathbb{R})$ since the convergence of the finite-difference approximations of the first and second partial derivatives of the function I_1 can be estimated by the mesh size.

[37] In order to make the convergence theorem from [Franek/Franek/Maurer/Wagner 10] applicable to the y-component of the solutions as well, one had to assume e. g. $y \in W_0^{1,\infty}(\Omega,\mathbb{R})$ together with an additional gradient constraint $\| \nabla y \| \leqslant \widetilde{R}$.

4. Evaluation and visualization of the solutions; image data.

a) Evaluation and visualization of the solutions.

After a minimizing solution $(\hat{x}, \hat{y})$ of $(\mathrm{P})_{lin}$ or $(\mathrm{P})_{hyp}$ has been determined, we calculate

$$I_{rek}(s) \;=\; I_1(s) \;-\; DI_1(s)^{\mathrm{T}}\,\hat{x}(s) \;+\; \tfrac{1}{2}\,\hat{x}(s)^{\mathrm{T}}\,D^2I_1(s)\,\hat{x}(s) \;+\; \tfrac{1}{6}\,\hat{y}(s)\cdot\|\,\hat{x}(s)\,\|^3 \tag{4.1}$$

as the according reconstruction of the reference image I_0. In order to perform a quantitative evaluation of the results, we will measure the relative reconstruction error

$$Q(\hat{x},\hat{y}) \;=\; \left(\frac{\displaystyle\int_{\Omega\setminus\Omega_R} \Big(I_{rek}(s) - I_0(s) \Big)^2\,ds}{\displaystyle\int_{\Omega\setminus\Omega_R} \Big(I_1(s) \;\; - I_0(s) \Big)^2\,ds} \right)^{1/2} . \tag{4.2}$$

The influence of the remainder $\frac{1}{6}\,\hat{y}(s)\cdot\|\,\hat{x}(s)\,\|^3$, which will be interpreted as a grey value correction, can be quantified by means of the indicator

$$G(\hat{x},\hat{y}) \;=\; \operatorname*{Max}_{s\,\in\,\Omega\setminus\Omega_R} \Big|\, \tfrac{1}{6}\,\hat{y}(s)\cdot\|\,\hat{x}(s)\,\|^3 \,\Big| . \tag{4.3}$$

For the calculation of Q and G, a frame Ω_R dyed in black of 4 pixels width has been excluded.
In the present paper, the results of an elastic image registration will be visualized by a deformed grid showing the effect of the solution $\hat{x}$ when applied to a reference configuration (see e. g. Fig. 13) as well as by a colorful orientation plot.[38] Here the direction of the deformation vector is coded by the color of a pixel, while its intensity increases with the magnitude of the vector. The correspondence between orientation and color can be read from the colored border as a legend (see e. g. Fig. 12). The visualization has been realized using a HSI color model[39] where every color is represented by the three coordinates hue, saturation and intensity. Since we need only two coordinates for the visualization of the deformation field $\hat{x}$, the saturation has been left constant.
Besides $\hat{x}$, we document the grey value correction $\big|\, \frac{1}{6}\,\hat{y}(s)\cdot\|\,\hat{x}(s)\,\|^3 \,\big|$, where the correspondence of the greyscale values has been inverted (white corresponds to zero) and magnified by the factor 3 (see e. g. Fig. 17). In these figures, a frame of 4 pixels width has been dyed in grey.

b) Image data used in the experiments.

For our numerical experiments, four pairs of test images have been chosen, all originating from medical imaging. The first pair (Figs. 1 and 2) shows the kidney region.[40] The images have been consecutively generated via MR tomography with an interval of 2.4 seconds. The second pair (Figs. 3 and 5) is a cut-out of the first showing a coronal section through the left kidney; moreover, in the left half of the images, a part of the spine is visible. The original data have been presmoothed by (3×3)-averaging.
In the third and fourth pair, adjacent sections through the upper part of the body (heart region) are shown; the third pair (Figs. 6 and 8) has been generated via MR tomography and the fourth (Figs. 9 and 11) via

[38] Cf. [Brune/Maurer/Wagner 09], p. 1197 f.

[39] [Plataniotis/Venetsanopoulos 00], pp. 25 ff.

[40] Images courtesy of Prof. R. Stollberger (TU Graz, Institute of Medical Engineering) and Dr. M. Aschauer (Medical University of Graz, Division of Vascular and Interventional Radiology). From a contrast-modulated sequence comprising 135 frames in total, the frames #50 and #51 (with nearly identical modality) have been selected.

PE tomography. [41)] Before processing, the original data have been calibrated with respect to intensity and contrast and smoothed by (3×3)-averaging.
Additionally, in order to illustrate the effect of the greyscale value correction in an extreme case, we consider a synthetically generated fifth pair of binary images where the uppercase letters I and E should be matched (Figs. 61 and 62).
The first image pair has the size of 512×512 pixels; the sizes of the pairs $2-5$ amount to 128×128 pixels with a frame of 4 pixels width dyed in black, respectively.

Image pair 1: MR tomography of the kidney region.

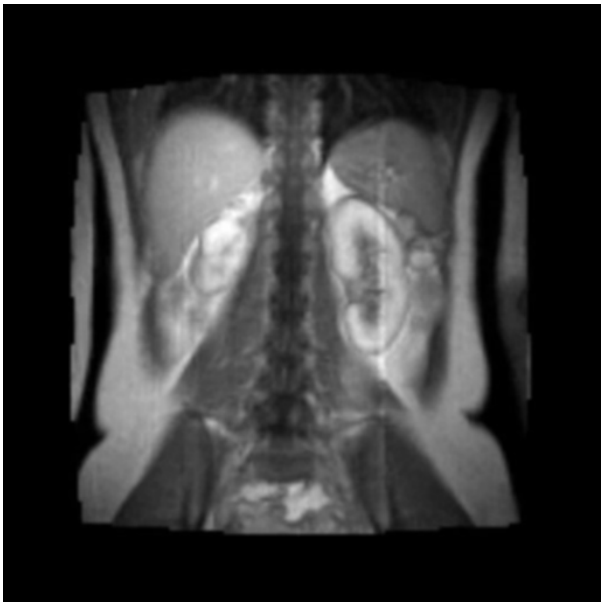

Fig. 1: Template I_1

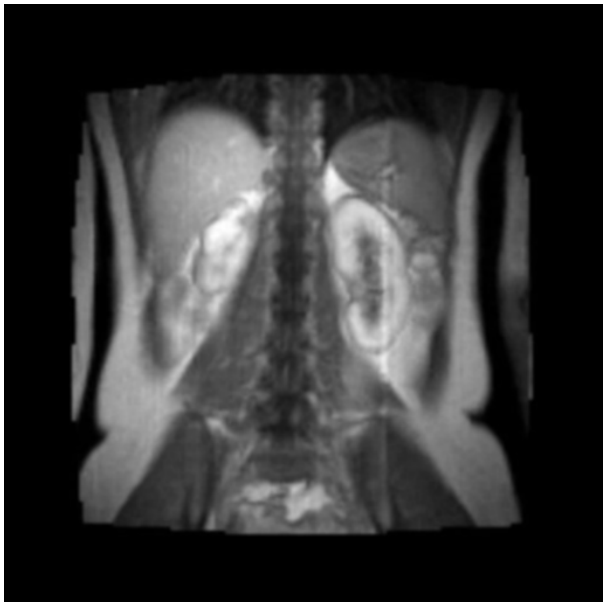

Fig. 2: Reference image I_0

Maximal grey value difference: $\mathrm{Max}_{s \in \Omega} \, | I_1(s) - I_0(s) | = 0.1529$

[41)] Images courtesy of Dr. M. Dawood (University of Münster, European Institute of Molecular Imaging), cf. [Dawood/Büther/Lang/Schober/Schäfers 07]. From two unimodal sequences with mutually coinciding image planes, the frames #29 and #30 have been selected, respectively.

Image pair 2: MR tomography of the kidney region, cut-out.

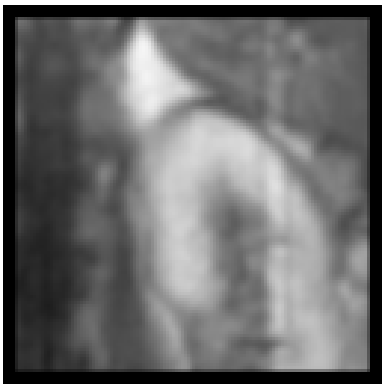

Fig. 3: Template I_1

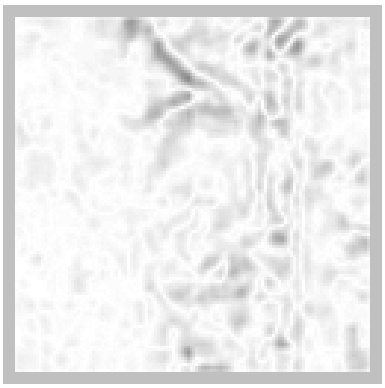

Fig. 4: Grey value difference $|\, I_1 - I_0 \,|$

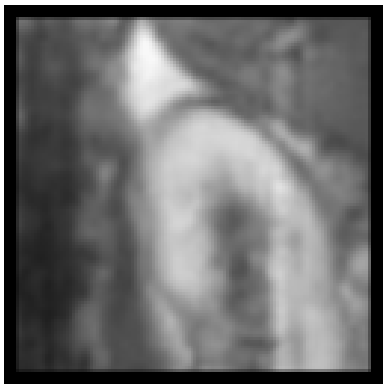

Fig. 5: Reference image I_0

Maximal grey value difference: $\mathrm{Max}_{\,s \in \Omega} \,|\, I_1(s) - I_0(s) \,| = 0.1529$

Image pair 3: MR tomography of the upper part of the body.

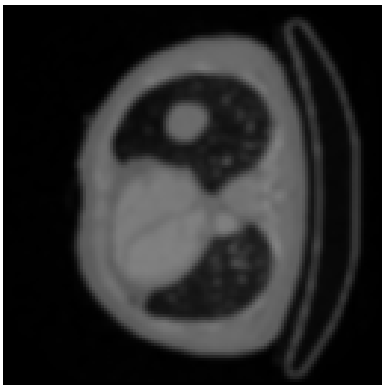

Fig. 6: Template I_1

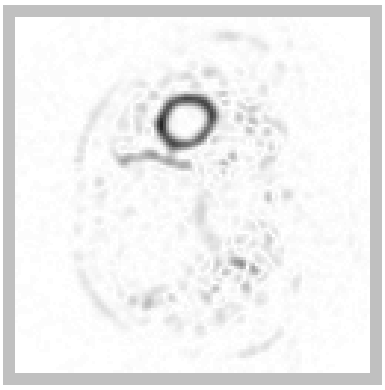

Fig. 7: Grey value difference $|\, I_1 - I_0 \,|$

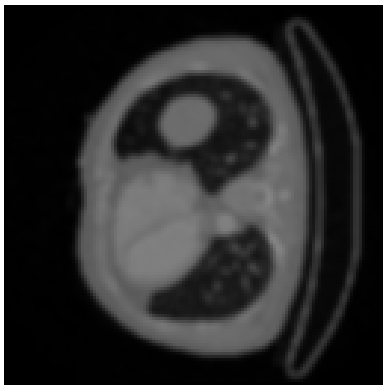

Fig. 8: Reference image I_0

Maximal grey value difference: $\mathrm{Max}_{\,s \in \Omega} \,|\, I_1(s) - I_0(s) \,| = 0.2862$

Image pair 4: PE tomography of the upper part of the body.

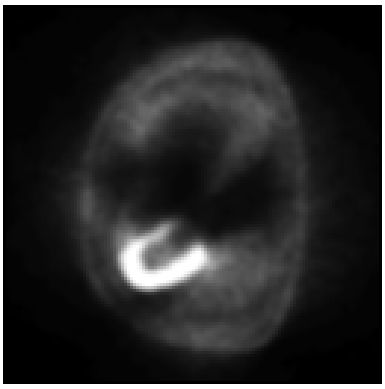

Fig. 9: Template I_1

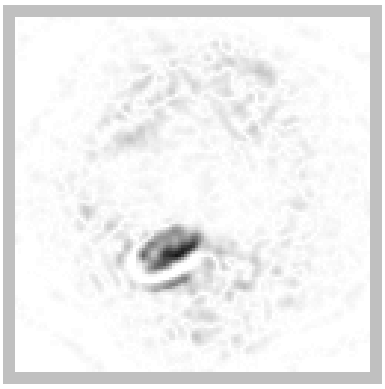

Fig. 10: Grey value difference $|\, I_1 - I_0 \,|$

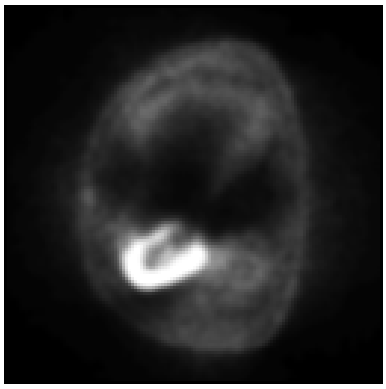

Fig. 11: Reference image I_0

Maximal grey value difference: $\mathrm{Max}_{\,s \in \Omega} \,|\, I_1(s) - I_0(s) \,| = 0.3019$

5. Numerical results.

a) Overview of the experiments.

In the following Subsection b), we document first the results with the best reconstruction quality Q for the image pairs $1-4$. In Subsection c), with the help of the image pairs $2-4$, we study the influence of the regularization parameters μ and R on the solutions while η_{max} has been left constant. Conversely, in Subsection d) the parameter η_{max} will be varied while μ and R remain unchanged. Here we use the image pairs 2, 4 and 5. Subsection e) contains experiments with inclusion of additional constraints. We present experiments with landmarks as well as with undistorted or purely translated subregions, respectively. Finally, a detailed discussion of the results will be provided in Subsection f).

b) Best results.

In the first table, the results with the best reconstruction quality Q will be listed.

	Image pair 1	Image pair 2	Image pair 3	Image pair 4
$(\mathrm{P})_{lin}$	$Q = 16.7729$ [a)] *$G = 0.2334$* $\mu = 10^{-6}$, $R = 12$, $\eta_{max} = 0.001$	$Q = 12.1556$ *$G = 0.1653$* $\mu = 10^{-5}$, $R = 2$, $\eta_{max} = 1.0$	$Q = 10.5367$ *$G = 0.4434$* $\mu = 10^{-6}$, $R = 12$, $\eta_{max} = 0.001$	$Q = 12.0505$ *$G = 0.1164$* $\mu = 10^{-6}$, $R = 10^3$, $\eta_{max} = 0.001$
$(\mathrm{P})_{hyp}$	$Q = 12.3228$ [b)] *$G = 0.3944$* $\mu = 10^{-6}$, $R = 12$, $\eta_{max} = 0.001$	$Q = 6.4187$ *$G = 0.2212$* $\mu = 10^{-5}$, $R = 2$, $\eta_{max} = 1.0$	$Q = 8.0546$ *$G = 0.5634$* $\mu = 10^{-6}$, $R = 10^3$, $\eta_{max} = 0.001$	$Q = 6.7443$ *$G = 0.4245$* $\mu = 10^{-5}$, $R = 2$, $\eta_{max} = 1.0$

Table 5.1. Best results with arbitrary grey value correction. In $(\mathrm{P})_{hyp}$, $p = 2$, $c_1 = 0.05$, $c_2 = 0.25$ have been chosen.

If only those results are accepted where the grey value correction G is bounded by the maximal grey value difference $\mathrm{Max}_{s \in \Omega} \, | I_1(s) - I_0(s) |$of the respective image pair, we arrive at the following table:

	Image pair 1	Image pair 2	Image pair 3	Image pair 4
$(\mathrm{P})_{lin}$	$Q = 20.5599$ *$G = 0.0470$* $\mu = 10^{-6}$, $R = 10$, $\eta_{max} = 10^{-4}$	$Q = 12.7953$ *$G = 0.1356$* $\mu = 10^{-5}$, $R = 2$, $\eta_{max} = 0.1$	$Q = 15.5396$ [a)] *$G = 0.1437$* $\mu = 10^{-6}$, $R = 2$, $\eta_{max} = 0.001$	$Q = 12.0505$ *$G = 0.1164$* $\mu = 10^{-6}$, $R = 10^3$, $\eta_{max} = 0.001$
$(\mathrm{P})_{hyp}$	$Q = 15.8672$ *$G = 0.1137$* $\mu = 10^{-6}$,$R = 10$, $\eta_{max} = 10^{-4}$	$Q = 15.6321$ *$G = 0.1340$* $\mu = 10^{-5}$, $R = 4$, $\eta_{max} = 0.001$	$Q = 14.8844$ [b)] *$G = 0.1580$* $\mu = 10^{-6}$, $R = 2$, $\eta_{max} = 0.001$	$Q = 9.1671$ [c)] *$G = 0.2265$* $\mu = 10^{-6}$, $R = 10^4$, $\eta_{max} = 0.001$

Table 5.2. Best results, grey value correction bounded. In $(\mathrm{P})_{hyp}$, $p = 2$, $c_1 = 0.05$, $c_2 = 0.25$ have been chosen.

Remarks. Table 5.1.: a) See Figs. $12-13$. b) See Figs. $14-15$.
Table 5.2.: a) See Figs. $16-18$. b) See Figs. $19-21$. c) See Figs. $22-24$.

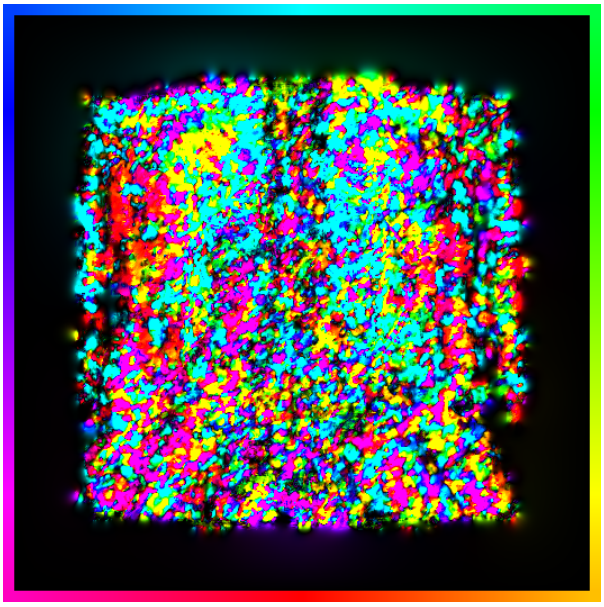

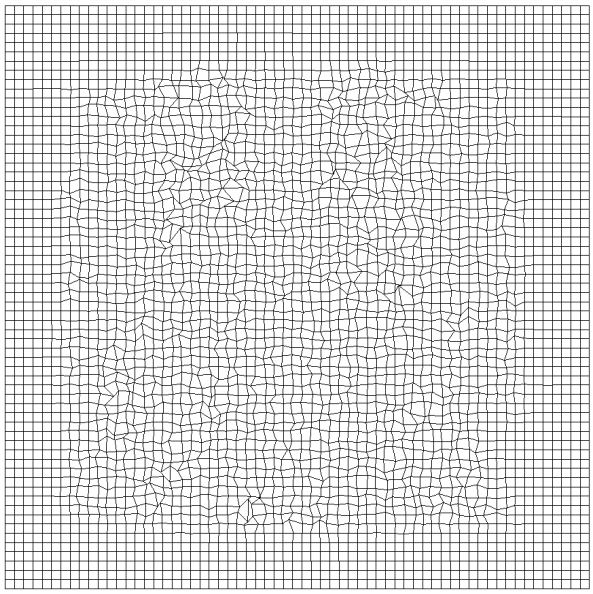

Figs. $12-13$: Results for $(\mathrm{P})_{lin}$ and image pair 1 with $\mu = 10^{-6}$, $R = 12$, $\eta_{max} = 0.001$

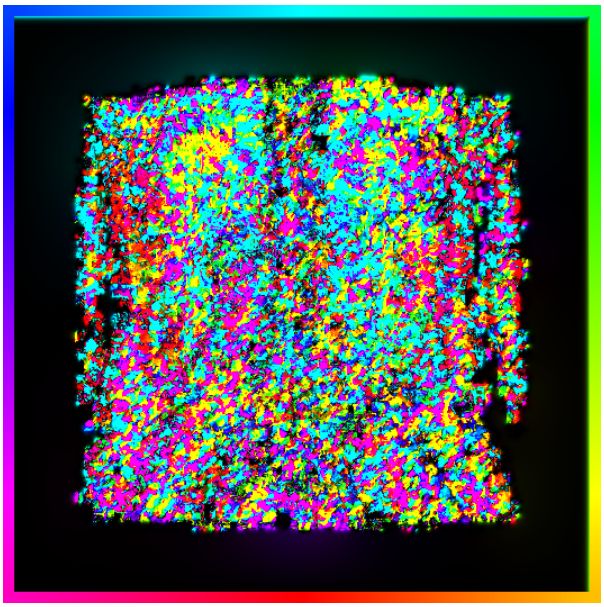

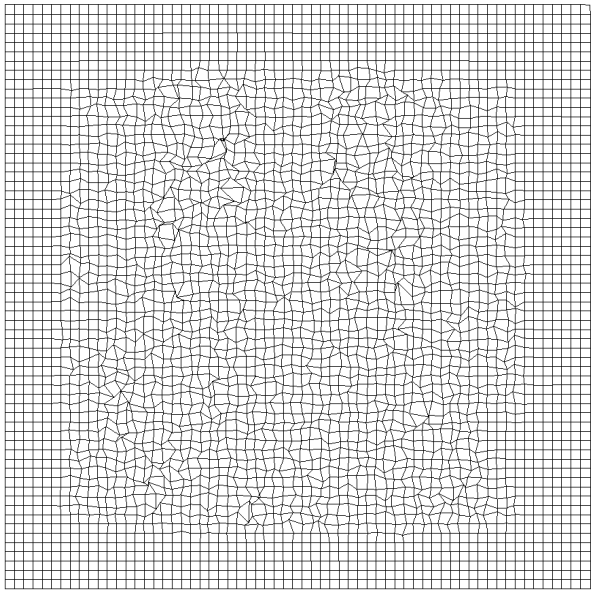

Figs. $14-15$: Results for $(\mathrm{P})_{hyp}$ and image pair 1 with $\mu = 10^{-6}$, $R = 12$, $\eta_{max} = 0.001$, $p = 2$, $c_1 = 0.05$, $c_2 = 0.25$

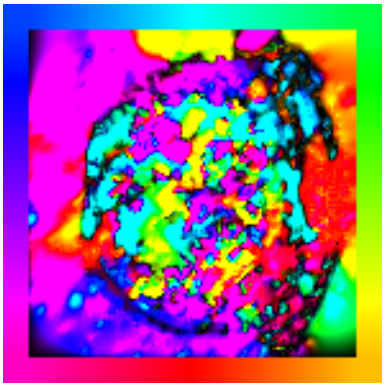

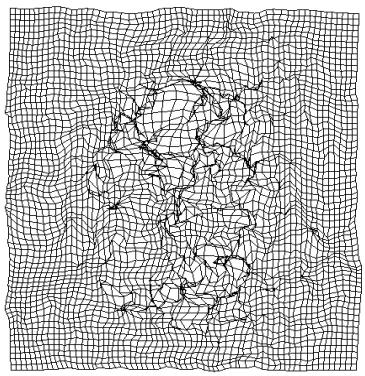

Figs. $16-18$: Results for $(\mathrm{P})_{lin}$ and image pair 3 with $\mu = 10^{-6}$, $R = 2$, $\eta_{max} = 0.001$

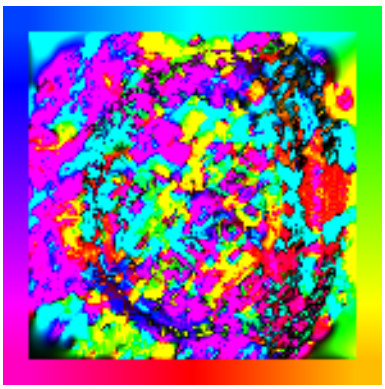

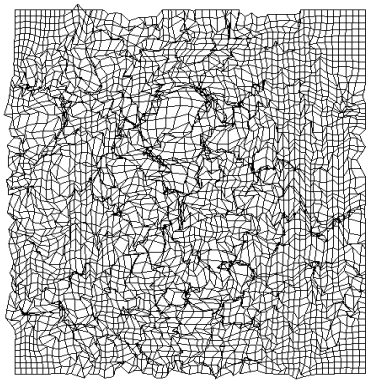

Figs. $19-21$: Results for $(\mathrm{P})_{hyp}$ and image pair 3 with $\mu = 10^{-6}$, $R = 2$, $\eta_{max} = 0.001$, $p = 2$, $c_1 = 0.05$, $c_2 = 0.25$

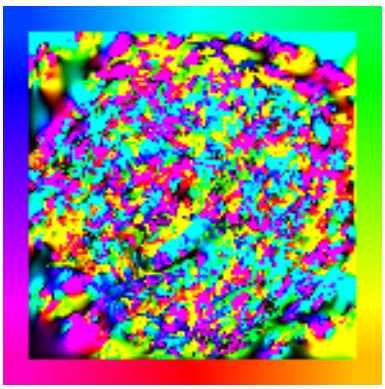

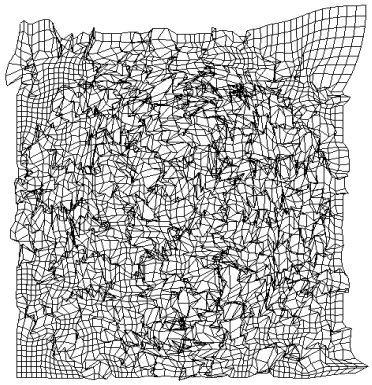

Figs. $22-24$: Results for $(\mathrm{P})_{hyp}$ and image pair 4 with $\mu = 10^{-6}$, $R = 10^4$, $\eta_{max} = 0.001$, $p = 2$, $c_1 = 0.05$, $c_2 = 0.25$

c) Influence of the parameters μ and R.

We provide three series of results with $\mu = 10^{-4}$, 10^{-5} and 10^{-6}, respectively, and variation in R.

	Image pair 2		Image pair 3		Image pair 4	
R	$(\mathrm{P})_{lin}$	$(\mathrm{P})_{hyp}$	$(\mathrm{P})_{lin}$	$(\mathrm{P})_{hyp}$	$(\mathrm{P})_{lin}$	$(\mathrm{P})_{hyp}$
0.25	$Q = 49.9918$	$Q = 48.9737$	$Q = 44.2981$	$Q = 43.4465$	$Q = 46.6049$	$Q = 45.4716$
	$G = 0.0092$	*$G = 0.0095$*	*$G = 0.0043$*	*$G = 0.0085$*	*$G = 0.0030$*	*$G = 0.0064$*
0.50	$Q = 41.4113$	$Q = 37.5695$	$Q = 32.5295$	$Q = 29.7263$	$Q = 37.7872$	$Q = 34.3152$
	$G = 0.0261$	*$G = 0.0333$*	*$G = 0.0139$*	*$G = 0.0173$*	*$G = 0.0135$*	*$G = 0.0235$*
1.00	$Q = 36.6221$	$Q = 28.1894$	$Q = 28.3317$	$Q = 21.8025$	$Q = 32.8227$	$Q = 25.7701$
	$G = 0.0291$	*$G = 0.0461$*	*$G = 0.0327$*	*$G = 0.0493$*	*$G = 0.0231$*	*$G = 0.0566$*
2.00	$Q = 35.3471$	$Q = 23.2602$	$Q = 27.5077$	$Q = 18.2080$	$Q = 31.1195$	$Q = 21.0237$
	$G = 0.0369$	*$G = 0.0817$*	*$G = 0.0344$*	*$G = 0.0801$*	*$G = 0.0245$*	*$G = 0.0543$*
4.00	$Q = 34.9750$	$Q = 20.5929$	$Q = 27.3403$	$Q = 15.8831$	$Q = 30.0015$	$Q = 17.0307$
	$G = 0.0381$	*$G = 0.0639$*	*$G = 0.0344$*	*$G = 0.0870$*	*$G = 0.0245$*	*$G = 0.0602$*
8.00	$Q = 34.9440$ [a)]	$Q = 19.1275$ [a)]	$Q = 27.3403$	$Q = 15.4135$ [a)]	$Q = 29.9762$	$Q = 16.6667$ [a)]
	$G = 0.0381$	*$G = 0.0748$*	*$G = 0.0344$*	*$G = 0.0822$*	*$G = 0.0245$*	*$G = 0.0599$*
12.00	$Q = 35.0476$	$Q = 19.2262$	$Q = 27.3403$	$Q = 15.4799$	$Q = 29.9762$	$Q = 16.6836$
	$G = 0.0381$	*$G = 0.0749$*	*$G = 0.0344$*	*$G = 0.0863$*	*$G = 0.0245$*	*$G = 0.0591$*
10^2	$Q = 35.0476$	$Q = 19.2275$	$Q = 27.3403$	$Q = 15.4993$	$Q = 29.9924$	$Q = 16.6973$
	$G = 0.0381$	*$G = 0.0749$*	*$G = 0.0344$*	*$G = 0.0822$*	*$G = 0.0245$*	*$G = 0.0591$*
10^3	$Q = 35.0476$	$Q = 19.2556$	$Q = 27.3403$	$Q = 15.5560$	$Q = 29.9762$	$Q = 16.6907$
	$G = 0.0381$	*$G = 0.0749$*	*$G = 0.0344$*	*$G = 0.0867$*	*$G = 0.0245$*	*$G = 0.0591$*
10^4	$Q = 35.0476$	$Q = 19.2534$	$Q = 27.3403$	$Q = 15.5560$	$Q = 29.9762$	$Q = 16.6935$
	$G = 0.0381$	*$G = 0.0749$*	*$G = 0.0344$*	*$G = 0.0867$*	*$G = 0.0245$*	*$G = 0.0591$*

Table 5.3. Variation in R for $\mu = 10^{-4}$, $\eta_{max} = 0.001$. In $(\mathrm{P})_{hyp}$, $p = 2$, $c_1 = 0.05$, $c_2 = 0.25$ have been chosen.

	Image pair 2		Image pair 3		Image pair 4	
R	$(\mathrm{P})_{lin}$	$(\mathrm{P})_{hyp}$	$(\mathrm{P})_{lin}$	$(\mathrm{P})_{hyp}$	$(\mathrm{P})_{lin}$	$(\mathrm{P})_{hyp}$
0.25	$Q = 48.9990$	$Q = 48.9383$	$Q = 43.5012$	$Q = 43.3879$	$Q = 45.5130$	$Q = 45.4082$
	$G = 0.0095$	*$G = 0.0094$*	*$G = 0.0069$*	*$G = 0.0097$*	*$G = 0.0059$*	*$G = 0.0078$*
0.50	$Q = 37.7058$	$Q = 37.3267$	$Q = 29.9156$	$Q = 29.4502$	$Q = 34.5038$	$Q = 34.1488$
	$G = 0.0329$	*$G = 0.0353$*	*$G = 0.0171$*	*$G = 0.0190$*	*$G = 0.0230$*	*$G = 0.0211$*
1.00	$Q = 28.5688$ [b)]	$Q = 27.0127$ [f)]	$Q = 22.3028$	$Q = 20.8209$	$Q = 26.2620$	$Q = 24.7471$
	$G = 0.0506$	*$G = 0.0540$*	*$G = 0.0485$*	*$G = 0.0650$*	*$G = 0.0571$*	*$G = 0.0627$*
2.00	$Q = 23.8161$ [c)]	$Q = 20.0422$ [g)]	$Q = 18.7026$	$Q = 15.3226$	$Q = 21.9221$	$Q = 18.6256$
	$G = 0.0863$	*$G = 0.1028$*	*$G = 0.0530$*	*$G = 0.1515$*	*$G = 0.0755$*	*$G = 0.0772$*
4.00	$Q = 21.8626$ [d)]	$Q = 15.6321$ [h)]	$Q = 17.3287$	$Q = 11.8266$	$Q = 18.5002$	$Q = 12.7733$
	$G = 0.0917$	*$G = 0.1340$*	*$G = 0.0564$*	*$G = 0.3609$*	*$G = 0.0798$*	*$G = 0.0756$*
8.00	$Q = 20.9644$	$Q = 12.9902$	$Q = 16.9014$	$Q = 10.3899$	$Q = 18.1728$ [a)]	$Q = 11.4774$
	$G = 0.0917$	*$G = 0.1773$*	*$G = 0.0576$*	*$G = 0.5197$*	*$G = 0.0797$*	*$G = 0.0852$*
12.00	$Q = 21.0102$ [e)]	$Q = 12.9879$ [i)]	$Q = 16.8948$ [a)]	$Q = 10.1453$	$Q = 18.1807$	$Q = 11.3959$
	$G = 0.0916$	*$G = 0.1954$*	*$G = 0.0576$*	*$G = 0.5363$*	*$G = 0.0797$*	*$G = 0.0852$*
10^2	$Q = 20.9396$ [a)]	$Q = 12.9640$ [a)]	$Q = 16.9005$	$Q = 10.1064$ [a)]	$Q = 18.1938$	$Q = 11.4162$
	$G = 0.0916$	*$G = 0.1958$*	*$G = 0.0576$*	*$G = 0.5363$*	*$G = 0.0797$*	*$G = 0.0852$*
10^3	$Q = 21.0353$	$Q = 13.1150$	$Q = 16.9273$	$Q = 10.1680$	$Q = 18.1912$	$Q = 11.3725$
	$G = 0.0505$	*$G = 0.1958$*	*$G = 0.0576$*	*$G = 0.5365$*	*$G = 0.0797$*	*$G = 0.0852$*
10^4	$Q = 21.0353$	$Q = 13.1400$	$Q = 16.9273$	$Q = 10.1681$	$Q = 18.1912$	$Q = 11.3725$
	$G = 0.0505$	*$G = 0.1958$*	*$G = 0.0576$*	*$G = 0.5365$*	*$G = 0.0797$*	*$G = 0.0852$*

Table 5.4. Variation in R for $\mu = 10^{-5}$, $\eta_{max} = 0.001$. In $(\mathrm{P})_{hyp}$, $p = 2$, $c_1 = 0.05$, $c_2 = 0.25$ have been chosen.

	Image pair 2		Image pair 3		Image pair 4	
R	$(\mathrm{P})_{lin}$	$(\mathrm{P})_{hyp}$	$(\mathrm{P})_{lin}$	$(\mathrm{P})_{hyp}$	$(\mathrm{P})_{lin}$	$(\mathrm{P})_{hyp}$
0.25	$Q = 48.9387$ *$G = 0.0094$*	$Q = 48.9374$ *$G = 0.0094$*	$Q = 43.3888$ *$G = 0.0096$*	$Q = 43.3919$ *$G = 0.0100$*	$Q = 45.4101$ *$G = 0.0077$*	$Q = 45.4040$ *$G = 0.0090$*
0.50	$Q = 37.3353$ *$G = 0.0352$*	$Q = 37.3146$ *$G = 0.0353$*	$Q = 29.4695$ *$G = 0.0177$*	$Q = 29.4241$ *$G = 0.0233$*	$Q = 34.1623$ *$G = 0.0211$*	$Q = 34.1279$ *$G = 0.0211$*
1.00	$Q = 27.0690$ *$G = 0.0543$*	$Q = 26.9095$ *$G = 0.0547$*	$Q = 20.9041$ *$G = 0.0631$*	$Q = 20.6848$ *$G = 0.0658$*	$Q = 24.8189$ *$G = 0.0630$*	$Q = 24.6250$ *$G = 0.0636$*
2.00	$Q = 20.1532$ *$G = 0.1045$*	$Q = 19.5233$ *$G = 0.1130$*	$Q = 15.5396$ [b)] *$G = 0.1437$*	$Q = 14.8844$ [c)] *$G = 0.1580$*	$Q = 18.7941$ *$G = 0.0967$*	$Q = 18.1035$ *$G = 0.0791$*
4.00	$Q = 15.7368$ *$G = 0.1436$*	$Q = 14.1965$ *$G = 0.2002$*	$Q = 12.0729$ *$G = 0.3167$*	$Q = 10.5557$ *$G = 0.3857$*	$Q = 13.0631$ *$G = 0.1241$*	$Q = 11.3006$ *$G = 0.0874$*
8.00	$Q = 13.2110$ *$G = 0.1514$*	$Q = 10.4685$ *$G = 0.2294$*	$Q = 10.6423$ *$G = 0.4307$*	$Q = 8.4046$ *$G = 0.5683$*	$Q = 12.0767$ *$G = 0.1077$*	$Q = 9.3802$ *$G = 0.2198$*
12.00	$Q = 13.2374$ *$G = 0.1500$*	$Q = 10.3440$ *$G = 0.2688$*	$Q = 10.5367$ [a)] *$G = 0.4434$*	$Q = 8.1045$ *$G = 0.5637$*	$Q = 12.0692$ *$G = 0.1164$*	$Q = 9.2450$ *$G = 0.2265$*
10^2	$Q = 13.1570$ [a)] *$G = 0.1500$*	$Q = 10.2129$ [a)] *$G = 0.2696$*	$Q = 10.6591$ *$G = 0.4378$*	$Q = 8.0843$ *$G = 0.5632$*	$Q = 12.0568$ *$G = 0.1164$*	$Q = 9.1749$ *$G = 0.2265$*
10^3	$Q = 13.2947$ *$G = 0.1500$*	$Q = 10.6609$ *$G = 0.2775$*	$Q = 10.6495$ *$G = 0.4378$*	$Q = 8.0546$ [a)] *$G = 0.5634$*	$Q = 12.0505$ *$G = 0.1164$*	$Q = 9.1679$ *$G = 0.2265$*
10^4	$Q = 13.2946$ *$G = 0.1500$*	$Q = 10.4558$ *$G = 0.2909$*	$Q = 10.6452$ *$G = 0.4378$*	$Q = 8.0552$ *$G = 0.5634$*	$Q = 12.0505$ *$G = 0.1164$*	$Q = 9.1671$ [d)] *$G = 0.2265$*

Table 5.5. Variation in R for $\mu = 10^{-6}$, $\eta_{max} = 0.001$. In $(\mathrm{P})_{hyp}$, $p = 2$, $c_1 = 0.05$, $c_2 = 0.25$ have been chosen.

Remarks. Table 5.3.: a) Best result of the column has been obtained with $R < 10^4$.
Table 5.4.: a) Best result of the column has been obtained with $R < 10^4$. b) See Figs. $25 - 27$. c) See Figs. $28 - 30$. d) See Figs. $31 - 33$. e) See Figs. $34 - 36$. f) See Figs. $37 - 39$. g) See Figs. $40 - 42$. h) See Figs. $43 - 45$. i) See Figs. $46 - 48$.
Table 5.5.: a) Best result of the column has been obtained with $R < 10^4$. b) See Figs. $16 - 18$. c) See Figs. $19 - 21$. d) See Figs. $22 - 24$.

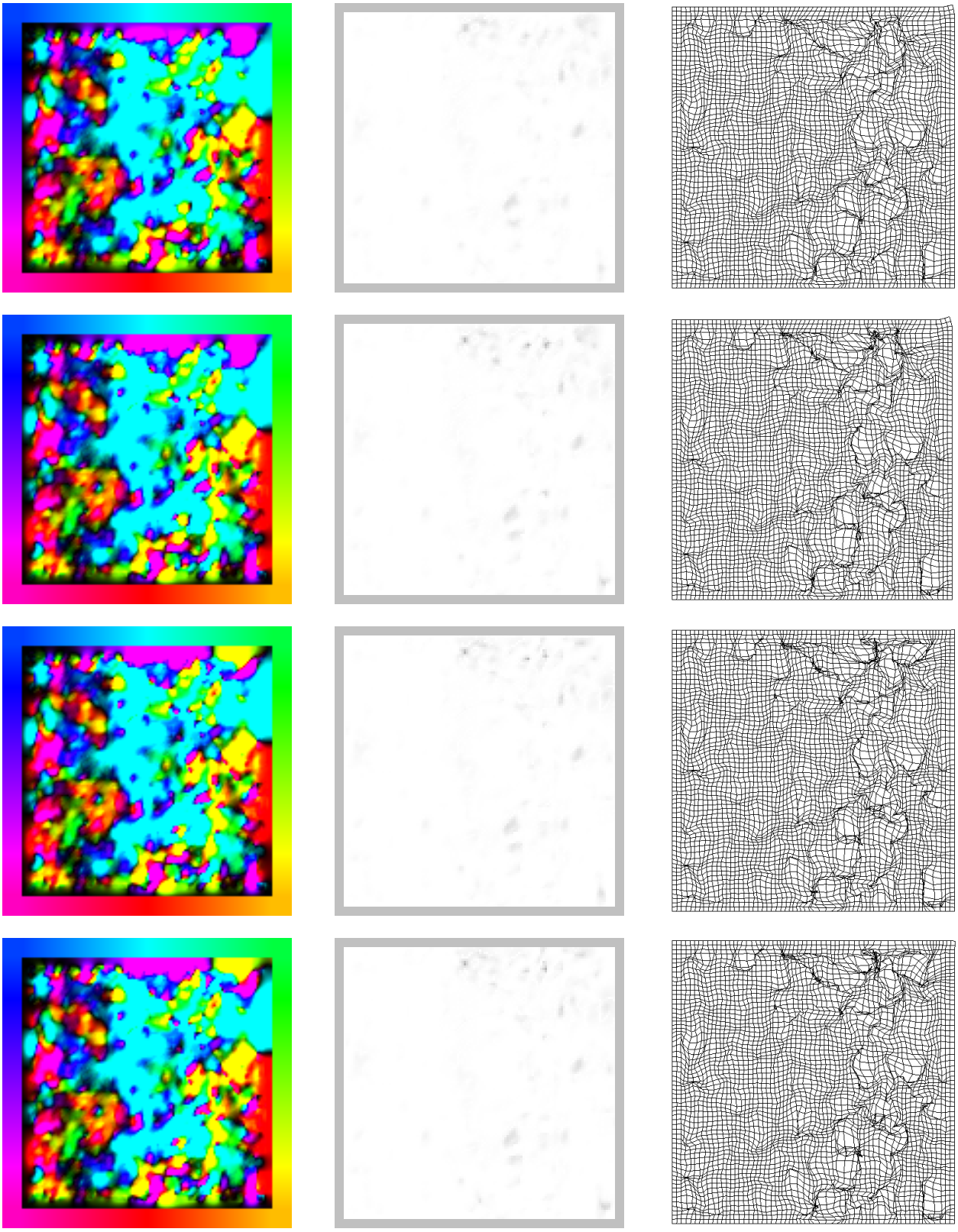

Figs. $25-36$: Results for $(\mathrm{P})_{lin}$ and image pair 2 with $\mu = 10^{-5}$, $\eta_{max} = 0.001$; variation in R.
First row: $R = 1$, second row: $R = 2$, third row: $R = 4$, fourth row: $R = 12$.

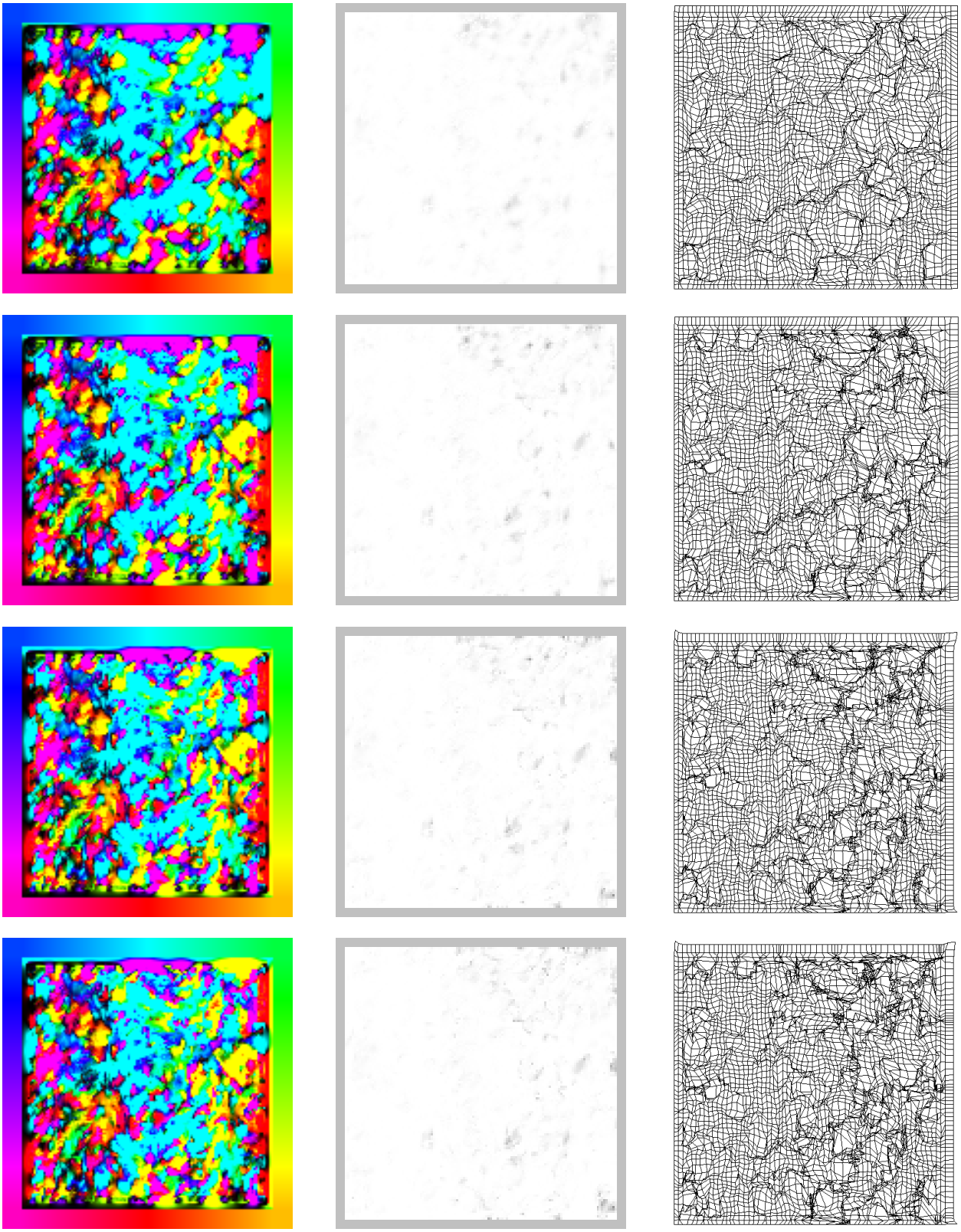

Figs. $37-48$: Results for $(\mathrm{P})_{hyp}$ and image pair 2 with $\mu = 10^{-5}$, $\eta_{max} = 0.001$, $p = 2$, $c_1 = 0.05$, $c_2 = 0.25$; variation in R. First row: $R = 1$, second row: $R = 2$, third row: $R = 4$, fourth row: $R = 12$.

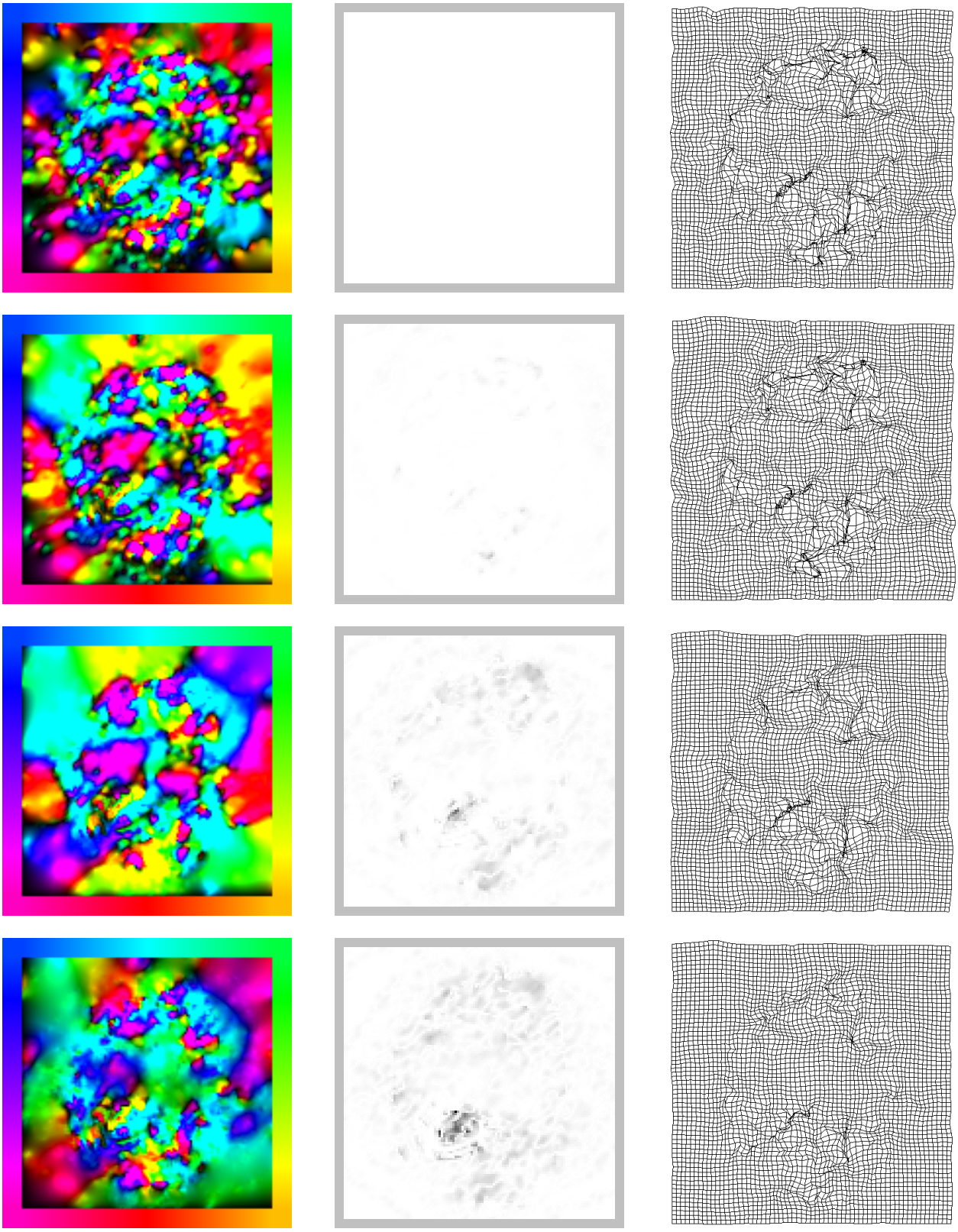

Figs. $49-60$: Results for $(\mathrm{P})_{lin}$ and image pair 4 with $R=2$, $\mu=10^{-5}$; variation in η_{max}.
First row: $\eta_{max}=0$, second row: $\eta_{max}=10^{-3}$, third row: $\eta_{max}=10^{-2}$, fourth row: $\eta_{max}=10^{-1}$.

d) Influence of the parameter η_{max}.

	Image pair 2		Image pair 4		Image pair 5	
η_{max}	$(\mathrm{P})_{lin}$	$(\mathrm{P})_{hyp}$	$(\mathrm{P})_{lin}$	$(\mathrm{P})_{hyp}$	$(\mathrm{P})_{lin}$	$(\mathrm{P})_{hyp}$
0	$Q = 28.0140$ *$G = 0$*	$Q = 24.6007$ *$G = 0$*	$Q = 23.8688$ [a)] *$G = 0$*	$Q = 20.7963$ *$G = 0$*	$Q = 94.4095$ *$G = 0$*	$Q = 94.4095$ *$G = 0$*
10^{-6}	$Q = 28.0096$ *$G = 0.0001$*	$Q = 24.6160$ *$G = 0.0001$*	$Q = 23.8789$ *$G = 0.0000$*	$Q = 20.7878$ *$G = 0.0000$*	$Q = 89.1241$ *$G = 0.2526$*	$Q = 89.1233$ *$G = 0.2526$*
10^{-5}	$Q = 27.9602$ *$G = 0.0012$*	$Q = 24.5253$ *$G = 0.0017$*	$Q = 23.8463$ *$G = 0.0004$*	$Q = 20.7400$ *$G = 0.0006$*	$Q = 63.5336$ *$G = 1.0000$*	$Q = 63.5330$ *$G = 1.0000$*
10^{-4}	$Q = 27.5452$ *$G = 0.0110$*	$Q = 24.0231$ *$G = 0.0160$*	$Q = 23.6845$ *$G = 0.0048$*	$Q = 20.5129$ *$G = 0.0099$*	$Q = 39.3174$ *$G = 1.0000$*	$Q = 39.3172$ *$G = 1.0000$*
10^{-3}	$Q = 23.8161$ *$G = 0.0863$*	$Q = 20.0422$ *$G = 0.1028$*	$Q = 21.9221$ [b)] *$G = 0.0755$*	$Q = 18.6256$ *$G = 0.0772$*	$Q = 29.8742$ *$G = 1.1041$*	$Q = 29.8741$ *$G = 1.1052$*
10^{-2}	$Q = 15.4305$ *$G = 0.1589$*	$Q = 10.9299$ *$G = 0.2253$*	$Q = 16.3550$ [c)] *$G = 0.1864$*	$Q = 12.4281$ *$G = 0.2516$*	$Q = 24.2592$ *$G = 1.1948$*	$Q = 24.2075$ *$G = 1.1099$*
10^{-1}	$Q = 12.7953$ *$G = 0.1356$*	$Q = 7.5963$ *$G = 0.2095$*	$Q = 12.9707$ [d)] *$G = 0.3326$*	$Q = 7.8480$ *$G = 0.4218$*	$Q = 22.5748$ *$G = 1.6189$*	$Q = 22.5837$ *$G = 1.6199$*
1	$Q = 12.1556$ *$G = 0.1653$*	$Q = 6.4187$ *$G = 0.2212$*	$Q = 12.1770$ *$G = 0.2783$*	$Q = 6.7443$ *$G = 0.4245$*	$Q = 22.2051$ *$G = 1.8859$*	$Q = 22.2050$ [e)] *$G = 1.8923$*

Table 5.6. Variation in η_{max} for $R = 2$, $\mu = 10^{-5}$. In $(\mathrm{P})_{hyp}$, $p = 2$, $c_1 = 0.05$, $c_2 = 0.25$ have been chosen.

Remark. a) See Figs. 49 – 51. b) See Figs. 52 – 54. c) See Figs. 55 – 57. d) See Figs. 58 – 60. e) See Figs. 63 – 66.

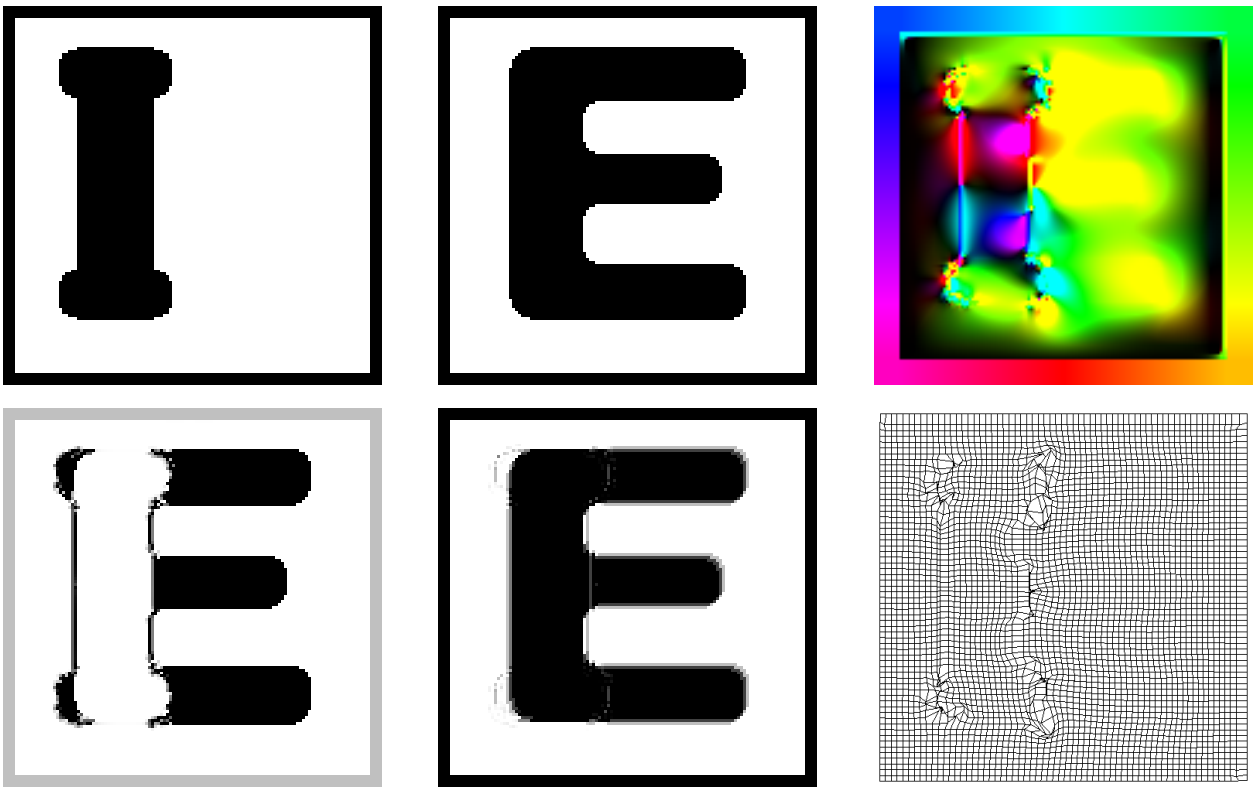

Figs. 61 – 66: Results for $(\mathrm{P})_{hyp}$ and image pair 5 with $\mu = 10^{-6}$, $R = 2$, $\eta_{max} = 1$, $p = 2$, $c_1 = 0.05$, $c_2 = 0.25$. From above and left: Template I_1, reference image I_0, $\hat{x}$ as colorplot, grey value difference, reconstruction I_{rek} of the reference image and grid deformed by $\hat{x}$.

e) Experiments with additional constraints.

We present three experiments where within the optimal control problems $(\mathrm{P})_{lin}$ and $(\mathrm{P})_{hyp}$, additional constraints according to Subsection 2.c) have been included. In the first experiment, we generated edge sketches for the image pair 3 (Figs. 67 and 68).[42] With the help of these sketches, the following landmarks have been brought in correspondence:

k	1	2	3	4	5	6	7	8	9
s_k (in I_1)	(37,75)	(49,77)	(55,74)	(63,73)	(71,64)	(55,88)	(62,82)	(70,90)	(62,95)
$\tilde{s}_k$ (in I_0)	(38,76)	(49,78)	(55,75)	(63,74)	(70,64)	(52,87)	(61,80)	(72,92)	(63,98)
$x(s_k)$	$\binom{-1}{-1}$	$\binom{0}{-1}$	$\binom{0}{-1}$	$\binom{0}{-1}$	$\binom{1}{0}$	$\binom{3}{1}$	$\binom{1}{2}$	$\binom{-2}{-2}$	$\binom{-1}{-3}$

Table 5.7. Landmarks for the constraints (2.8) in image pair 3

Accordingly, nine constraints of the shape (2.8) have been added to $(\mathrm{P})_{lin}$ and $(\mathrm{P})_{hyp}$. The second experiment has been performed with image pair 3 as well. Here we add a constraint (2.9) on the rectangular subregion $\Theta = [\,105\,,\,122\,] \times [\,5\,,\,124\,]$ (Fig. 69). This subregion contains the contours of the rack, whose position does not change in the images. In a third experiment with the constraint (2.10), we use the image pair 2. After a visual comparison of the images it has been presumed that the subregion $\Theta = \Theta_1 \cup \Theta_2$ with $\Theta_1 = [\,47\,,\,52\,] \times [\,100\,,\,110\,]$, $\Theta_2 = [\,55\,,\,63\,] \times [\,63\,,\,77\,]$ (Fig. 70) is subjected to a pure translation.

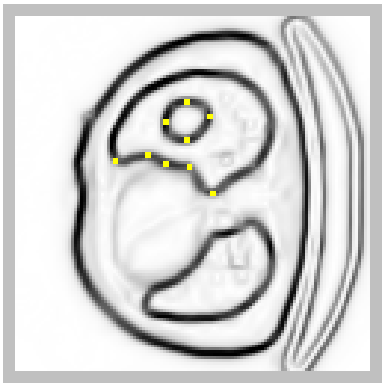

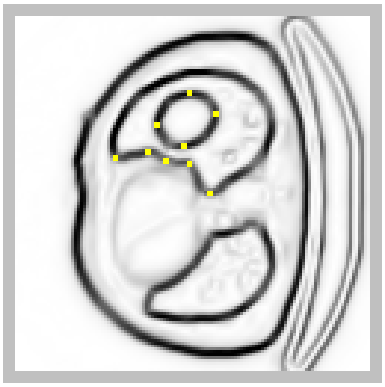

Figs. $67-68$: Edge sketches for I_1 (left) and I_0 (right) with landmarks (yellow)

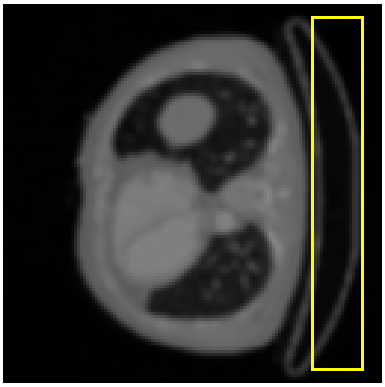

Fig. 69: Image pair 3: immotile subregion Θ (yellow border)

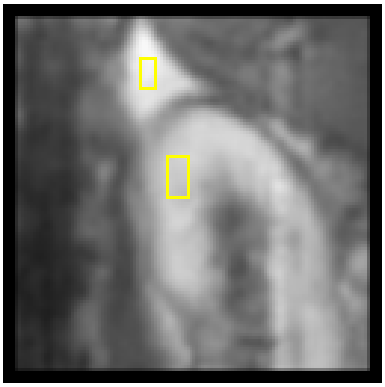

Fig. 70: Image pair 2: Subregion $\Theta = \Theta_1 \cup \Theta_2$ with pure translation (yellow border)

[42] By use of the optimal control method described in [Franek/Franek/Maurer/Wagner 10], p. 13.

The results have been assembled in the following table::

	Image pair 3 no constr.	Image pair 3 (2.8)	Image pair 3 (2.9)	Image pair 2 no constr.	Image pair 2 (2.10)
$(\mathrm{P})_{lin}$	$Q = 16.9014$ [a)] *$G = 0.0576$* $\mu = 10^{-5}$, $R = 8$, $\eta_{max} = 0.001$	$Q = 17.5100$ [b)] *$G = 0.0575$* $\mu = 10^{-5}$, $R = 8$, $\eta_{max} = 0.001$	$Q = 17.6469$ [c)] *$G = 0.0529$* $\mu = 10^{-5}$, $R = 8$, $\eta_{max} = 0.001$ $\varepsilon = 10^{-6}$	$Q = 15.4305$ [d)] *$G = 0.1589$* $\mu = 10^{-5}$, $R = 2$, $\eta_{max} = 0.01$	$Q = 15.3176$ [e)] *$G = 0.1597$* $\mu = 10^{-5}$, $R = 2$, $\eta_{max} = 0.01$ $\varepsilon = 10^{-3}$
$(\mathrm{P})_{hyp}$	$Q = 10.3899$ *$G = 0.5197$* $\mu = 10^{-5}$, $R = 8$, $\eta_{max} = 0.001$	$Q = 11.1837$ *$G = 0.5362$* $\mu = 10^{-5}$, $R = 8$, $\eta_{max} = 0.01$	$Q = 11.5735$ *$G = 0.5361$* $\mu = 10^{-5}$, $R = 8$, $\eta_{max} = 0.001$ $\varepsilon = 10^{-6}$	$Q = 10.9299$ *$G = 0.2253$* $\mu = 10^{-5}$, $R = 2$, $\eta_{max} = 0.01$	$Q = 10.3687$ *$G = 0.2321$* $\mu = 10^{-5}$, $R = 2$, $\eta_{max} = 0.001$ $\varepsilon = 10^{-3}$

Table 5.8. Experiments including additional constraints. In $(\mathrm{P})_{hyp}$, $p = 2$, $c_1 = 0.05$, $c_2 = 0.25$ have been chosen.

Remarks. a) See Figs. 77 – 79. b) See Figs. 80 – 82. c) See Figs. 83 – 85. d) See Figs. 71 – 73. e) See Figs. 74 – 76.

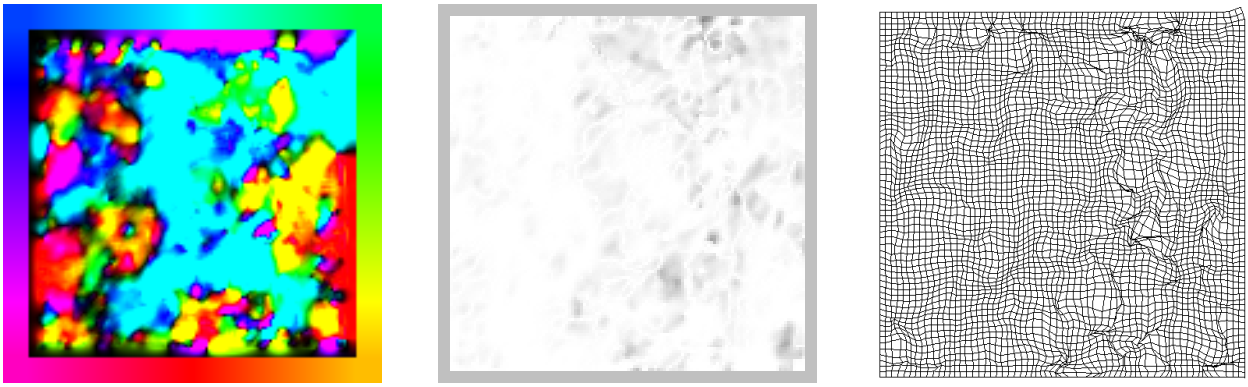

Figs. 71 – 73: Results for $(\mathrm{P})_{lin}$ and image pair 2, experiment without additional constraints for comparison: $\mu = 10^{-5}$, $R = 2$, $\eta_{max} = 0.01$

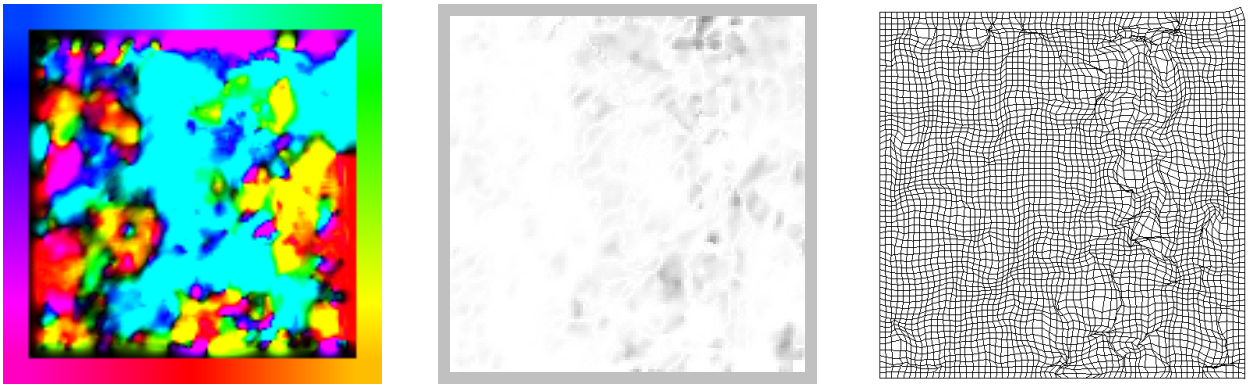

Figs. 74 – 76: Results for $(\mathrm{P})_{lin}$ and image pair 2, experiment with pure translation of the subregion $\Theta_1 \cup \Theta_2$: $\mu = 10^{-5}$, $R = 2$, $\eta_{max} = 0.01$, $\varepsilon = 0.001$

Figs. 77 – 79: Results for $(\mathrm{P})_{lin}$ and image pair 3, experiment without additional constraints for comparison: $\mu = 10^{-5}$, $R = 8$, $\eta_{max} = 0.001$

Figs. 80 – 82: Results for $(\mathrm{P})_{lin}$ and image pair 3, experiment with landmarks: $\mu = 10^{-5}$, $R = 8$, $\eta_{max} = 0.001$

Figs. 83 – 85: Results for $(\mathrm{P})_{lin}$ and image pair 3, experiment with immotile subregion: $\mu = 10^{-5}$, $R = 8$, $\eta_{max} = 0.001$, $\varepsilon = 10^{-6}$

f) Discussion of the results.

In Subsections 5.b) and 5.c), the relative error has been reduced even for moderate values of the regularization parameter μ by 70%; with an appropriate choice of μ, η_{max} and R, registrations with relative errors of 10% and below can be obtained (the best value amounts to $Q = 6.7\%$).

Even when ruling out experiments where the grey value correction G exceeds the maximal grey value difference of the original images, the relative error can be reduced by $85-90\%$ (Tables 5.1. and 5.2.). It is remarkable that in all experiments, for identical values of μ, R and η_{max}, the hyperelastic regularization produces significantly better values of Q. On the contrary, as one may expect, the convex problem $(\mathrm{P})_{lin}$ is superior to the polyconvex problem $(\mathrm{P})_{hyp}$ with respect to the runtime behaviour. The mutual comparison between the data sets originating from different imaging methods shows that the variation of the parameters μ, R and η_{max} within the problems $(\mathrm{P})_{lin}$ and $(\mathrm{P})_{hyp}$ influences the results in a comparable way (Tables $5.3.-5.5.$).
The results of Subsection 5.c) demonstrate that indeed, in comparison with the (unconstrained) variational problems, the presence of a control restriction may slightly improve the registration quality (note that, for sufficiently large R, the global minimizers of the control problems $(\mathrm{P})_{lin}$ and $(\mathrm{P})_{hyp}$ are the same as for the variational problems $(\mathrm{V})_{lin}$ and $(\mathrm{V})_{hyp}$). The parameter R within the control restriction behaves like an additional regularization parameter.
The necessity of the introduction of the remainder term $\frac{1}{6}\, y(s)\cdot \| x(s) \|^3$ into the approximation of the fidelity term is strongly supported by the results of Subsection 5.d). When deactivating this member by $\eta_{max}=0$, one observes typically a loss of $3-5\%$ registration quality in comparison with $|\, y\,| \leqslant \eta_{max} = 10^{-3}$, and even a loss of more than 10% in comparison with $|\, y\,| \leqslant \eta_{max} = 10^{-2}$. Further, one may convince oneself that, for the data from medical imaging, the character of x as a linear-elastic or hyperelastic deformation has been conserved if the bound η_{max} ranges within $0.001 - 0.01$ (Table 5.6., columns $1-4$). On the other hand, the experiments with the image pair 5 illustrate a situation where a registration by an elastic deformation cannot be realized from the outset. Nevertheless, we arrive at results with a registration quality of about 25% for values of $\eta_{max} \geqslant 0.01$. In this situation, however, the brunt of the reconstruction is borne by the correction term ($G \geqslant 1$) while the deformation $\hat{x}$ makes only an inferior contribution.
The incorporation of additional constraints in Subsection 5.e) becomes important if, on the base of $\hat{x}$, conclusions about the actual motion of the pictured objects will be drawn. Then the motions known in advance should be replicated within $\hat{x}$. Our experiments show that the addition of state constraints and restrictions of the shape $(2.8)-(2.10)$ to the control problems causes no significant change of the registration quality (Table 5.8.). Due to the according reduction of the number of variables, the "freezing" of immotile subregions (constraint (2.9) with $\varepsilon = 0$) may be of numerical importance.

g) Conclusion and outlook.

In the present work, we demonstrated that the elastic/hyperelastic image registration problem can be successfully reformulated and solved as a multidimensional control problem. Within this framework, even an improvement of the registration quality could be observed in comparison with the respective variational problems. In our experiments, the relative error between template and reference image could be reduced in the course of the registration by up to 90%. In accordance with the requirements of the registration and the information a priori available, additional state and control restrictions can be introduced into the problems. Surely the present approach may be further developed and improved according to different viewpoints. This remark concerns the general modelling (e. g. different approximations for the fidelity term, a symmetrical modelling with respect to the roles of I_1 and I_0, or an additional regularization with respect to y), the discretization strategy (generation of an adaptive triangulation instead of an uniform one) as well as the implementation (optimization of the runtime behaviour, registration of three- or four-dimensional data stacks).
Finally, the results of the present paper open the prospect of an optimal control access to the multimodal image registration problem. The generalization of the numerical approach presented here and its combina-

tion with the achievements from [Franek/Franek/Maurer/Wagner 10] will be reserved for a future publication.

Acknowledgement.

At this point, I wish to thank particularly A. Angelov (Münster), K. Bredies (Graz), Prof. M. Fröhner (Cottbus), Prof. G. Holzapfel (Graz), Prof. S. Keeling (Graz), F. Kemm (Cottbus and Saarbrücken) and Prof. K. Kunisch (Graz) who contributed to the present work with helpful discussions as well as with practical advice. Further, I would like to thank Prof. R. Stollberger (Graz) and M. Aschauer (Graz) as well as M. Dawood (Münster) who kindly provided me with tomographic image data. Since September 2009, the author's work has been supported within the Special Research Unit "Mathematical Optimization and Applications in Biomedical Sciences" (Graz) by the Austrian Science Fund.

References.

1. [Alvarez/Weickert/Sánchez 00] Alvarez, L.; Weickert, J.; Sánchez, J.: *Reliable estimation of dense optical flow fields with large displacements.* Int. J. Computer Vision **39** (2000), 41 – 56
2. [Aubert/Kornprobst 06] Aubert, G.; Kornprobst, P.: *Mathematical Problems in Image Processing: Partial Differential Equations and the Calculus of Variations.* Springer; New York etc. 2006, 2nd ed.
3. [Ball 77] Ball, J. M.: *Convexity conditions and existence theorems in nonlinear elasticity.* Arch. Rat. Mech. Anal. **63** (1977), 337 – 403
4. [Balzani/Neff/Schröder/Holzapfel 06] Balzani, D.; Neff, P.; Schröder, J.; Holzapfel, G. A.: *A polyconvex framework for soft biological tissues. Adjustment to experimental data.* Int. J. of Solids and Structures **43** (2006), 6052 – 6070
5. [Barbieri/Welk/Weickert 09] Barbieri, S.; Welk, M.; Weickert, J.: *A variational approach to the registration of tensor-valued images.* In: Aja-Fernández, S.; de Luis-García, R.; Tao, D.; Li, X. (Eds.): Tensors in Image Processing and Computer Vision. Springer; London etc. 2009, 59 – 77
6. [Breitenreicher/Schnörr 09] Breitenreicher, D.; Schnörr, C.: *Robust 3D object registration without explicit correspondence using geometric integration.* Machine Vis. and Appl.; electronically published: http://dx.doi.org/10.1007/s00138-009-0227-6 (accessed at 01. 12. 2009)
7. [Brune/Maurer/Wagner 09] Brune, C.; Maurer, H.; Wagner, M.: *Detection of intensity and motion edges within optical flow via multidimensional control.* SIAM J. Imaging Sci. **2** (2009), 1190 – 1210
8. [Chmelka/Melan 76] Chmelka, F.; Melan, E.: *Einführung in die Festigkeitslehre.* Springer; Wien - New York 1976, 5th ed.
9. [Christensen/Rabbitt/Miller 96] Christensen, G. E.; Rabbitt, R. D.; Miller, M. I.: *Deformable templates using large deformation kinematics.* IEEE Trans. Image Processing **5** (1996), 1435 – 1447
10. [Dacorogna 08] Dacorogna, B.: *Direct Methods in the Calculus of Variations.* Springer; New York etc. 2008, 2nd ed.
11. [Dawood/Büther/Lang/Schober/Schäfers 07] Dawood, M.; Büther, F.; Lang, N.; Schober, O.; Schäfers, K. P.: *Respiratory gating in positron emission tomography: a quantitative comparision of different gating schemes.* Med. Phys. **34** (2007), 3067 – 3076
12. [Droske/Rumpf 04] Droske, M.; Rumpf, M.: *A variational approach to nonrigid morphological image registration.* SIAM J. Appl. Math. **64** (2004), 668 – 687
13. [Droske/Rumpf 07] Droske, M.; Rumpf, M.: *Multiscale joint segmentation and registration of image morphology.* IEEE Trans. Pattern Recognition Machine Intelligence **29** (2007), 2181 – 2194
14. [Dunford/Schwartz 88] Dunford, N.; Schwartz, J. T.: *Linear Operators. Part I: General Theory.* Wiley-Interscience; New York etc. 1988
15. [Evans/Gariepy 92] Evans, L. C.; Gariepy, R. F.: *Measure Theory and Fine Properties of Functions.* CRC Press; Boca Raton etc. 1992
16. [Faugeras/Hermosillo 04] Faugeras, O.; Hermosillo, G.: *Well-posedness of two nonrigid multimodal image registration methods.* SIAM J. Appl. Math. **64** (2004), 1550 – 1587

17. [Fischer/Modersitzki 03] Fischer, B.; Modersitzki, J.: *Curvature based image registration.* J. Math. Imaging Vision **18** (2003), 81 – 85
18. [Fourer/Gay/Kernighan 03] Fourer, R.; Gay, D. M.; Kernighan, B. W.: *AMPL. A Modeling Language for Mathematical Programming.* Brooks/Cole — Thomson Learning; Pacific Grove 2003, 2nd ed.
19. [Franek/Franek/Maurer/Wagner 10] Franek, L.; Franek, M.; Maurer, H.; Wagner, M.: *A discretization method for the numerical solution of Dieudonné-Rashevsky type problems with application to edge detection within noisy image data. Revised version.* KFU Graz, SFB-Report No. 2010–003. Submitted: Opt. Contr. Appl. Meth.
20. [Gallardo/Meju 03] Gallardo, L. A.; Meju, M. A.: *Characterization of heterogeneous near-surface materials by joint 2D inversion of dc resistivity and seismic data.* Geophysical Research Letters **30** (2003) 13, 1658, 1 - 1 – 1 - 4
21. [Gasser/Holzapfel 02] Gasser, T. C.; Holzapfel, G. H.: *A rate-independent elastoplastic constitutive model for biological fiber-reinforced composites at finite strains: continuum basis, algorithmic formulation and finite element implementation.* Computational Mechanics **29** (2002), 340 – 360
22. [Goering/Roos/Tobiska 93] Goering, H.; Roos, H.-G.; Tobiska, L.: *Finite-Element-Methode.* Akademie-Verlag; Berlin 1993, 3rd ed.
23. [Haber/Modersitzki 04] Haber, E.; Modersitzki, J.: *Numerical methods for volume preserving image registration.* Inverse Problems **20** (2004), 1621 – 1638
24. [Haber/Modersitzki 07a] Haber, E.; Modersitzki, J.: *Image registration with guaranteed displacement regularity.* Int. J. Computer Vision **71** (2007), 361 – 372
25. [Haber/Modersitzki 07b] Haber, E.; Modersitzki, J.: *Intensity gradient based registration and fusion of multimodal images.* Methods of Information in Medicine **46** (2007), 292 – 299
26. [Haker/Zhu/Tannenbaum/Angenent 04] Haker, S.; Zhu, L.; Tannenbaum, A.; Angenent, S.: *Optimal mass transport for registration and warping.* Int. J. Computer Vision **60** (2004), 225 – 240
27. [Henn/Witsch 00] Henn, S.; Witsch, K.: *A multigrid approach for minimizing a nonlinear functional for digital image matching.* Computing **64** (2000), 339 – 348
28. [Henn/Witsch 01] Henn, S.; Witsch, K.: *Iterative multigrid regularization techniques for image matching.* SIAM J. Sci. Comput. **23** (2001), 1077 – 1093
29. [Hermosillo/Chefd'hotel/Faugeras 02] Hermosillo, G.; Chefd'hotel, C.; Faugeras, O.: *Variational methods for multimodal image matching.* Int. J. Computer Vision **50** (2002), 329 – 343
30. [Hintermüller/Keeling 09] Hintermüller, M.; Keeling, S. L.: *Image registration and segmentation based on energy minimization.* In: Pardalos, P. M.; Romeijn, H. E. (Eds.): Handbook of Optimization in Medicine. Springer; New York 2009, 213 – 252
31. [Jansen 97] Jansen, B.: *Interior Point Techniques in Optimization.* Kluwer; Dordrecht 1997
32. [Kaijser 98] Kaijser, T.: *Computing the Kantorovich distance for images.* J. Math. Imaging Vision **9** (1998), 173 – 191
33. [Keeling/Ring 05] Keeling, S. L.; Ring, W.: *Medical image registration and interpolation by optical flow with maximal rigidity.* J. Math. Imaging Vision **23** (2005), 47 – 65
34. [Laird/Wächter 09] Laird, C.; Wächter, A.: *Introduction to IPOPT: A tutorial for downloading, installing, and using IPOPT. Revision No. 1597.* Electronically published: http://www.coin-or.org/Ipopt/documentation/ (accessed at 30. 11. 2009)
35. [Le Guyader/Vese 09] Le Guyader, C.; Vese, L.: *A combined segmentation and registration framework with a nonlinear elasticity smoother.* In: Tai, X.-C.; Mørken, K.; Lysaker, M.; Lie, K.-A. (Eds.): Scale Space and Variational Methods in Computer Vision, Second International Conference, SSVM 2009, Voss, Norway, June 1-5, 2009. Proceedings. Springer; Berlin - Heidelberg 2009 (LNCS 5567), 600 – 611
36. [Liao/Yu/Bergsneider/Vese/Huang 03] Liao, W-H.; Yu, C.-L.; Bergsneider, M.; Vese, L.; Huang, S-C.: *A new framework of quantifying differences between images by matching gradient fields and its application to image blending.* In: Metzler, S. (Ed.): 2002 IEEE Nuclear Science Symposium Conference Record, Vol. 2. IEEE; Piscataway 2003, 1092 – 1096
37. [Modersitzki 04] Modersitzki, J.: *Numerical Methods for Image Registration.* Oxford University Press; Oxford 2004
38. [Modersitzki 09] Modersitzki, J.: *FAIR. Flexible Algorithms for Image Registration.* SIAM; Philadelphia 2009
39. [Museyko/Stiglmayr/Klamroth/Leugering 09] Museyko, O.; Stiglmayr, M.; Klamroth, K.; Leugering, G.: *On the application of the Monge-Kantorovich problem to image registration.* SIAM J. Imaging Sci. **2** (2009), 1068 – 1097

40. [Ogden 03] Ogden, R. W.: *Nonlinear elasticity, anisotropy, material stability and residual stresses in soft tissue.* In: Holzapfel, G. A.; Ogden, R. W. (Eds.): Biomechanics of Soft Tissue in Cardiovascular Systems. Springer; Wien etc. 2003, 65 – 108

41. [Pickenhain/Wagner 00] Pickenhain, S.; Wagner, M.: *Critical points in relaxed deposit problems.* In: Ioffe, A.; Reich, S.; Shafrir, I. (Eds.): Calculus of Variations and Optimal Control, Technion 98, Vol. II (Research Notes in Mathematics, Vol. 411). Chapman & Hall / CRC Press; Boca Raton etc. 2000, 217 – 236

42. [Pöschl/Modersitzki/Scherzer 09] Pöschl, C.; Modersitzki, J.; Scherzer, O.: *A variational setting for volume constrained image registration.* NRN Report No. 83; University of Innsbruck 2009

43. [Plataniotis/Venetsanopoulos 00] Plataniotis, K. N.; Venetsanopoulos, A. N.: *Color Image Processing and Applications.* Springer; Berlin etc. 2000

44. [Scherzer/Grasmair/Grossauer/Haltmeier/Lenzen 09] Scherzer, O.; Grasmair, M.; Grossauer, H.; Haltmeier, M.; Lenzen, F.: *Variational Methods in Imaging.* Springer; New York etc. 2009

45. [Vemuri/Ye/Chen/Leonard 00] Vemuri, B. C.; Ye, J.; Chen, Y.; Leonard, C. M.: *A level-set based approach to image registration.* In: IEEE Workshop on Mathematical Methods in Biomedical Image Analysis (MMBIA'00). IEEE Computer Society; Washington 2000, 86 – 93

46. [Wächter/Biegler 06] Wächter, A.; Biegler, L. T.: *On the implementation of an interior-point filter line-search algorithm for large-scale nonlinear programming.* Math. Program. Ser. A **106** (2006), 25 – 57

47. [Wagner 06] Wagner, M.: *Mehrdimensionale Steuerungsprobleme mit quasikonvexen Integranden.* Habilitation thesis. Brandenburg University of Technology, Cottbus 2006

48. [Wagner 08] Wagner, M.: *Quasiconvex relaxation of multidimensional control problems with integrands $f(t, \xi, v)$.* Max-Planck-Institut für Mathematik in den Naturwissenschaften, Leipzig. Preprint 68/2008. Accepted for publication: ESAIM: Control, Optimisation and Calculus of Variations

49. [Wagner 09] Wagner, M.: *Pontryagin's maximum principle for multidimensional control problems in image processing.* J. Optim. Theory Appl. **140** (2009), 543 – 576

50. [Wagner 10] Wagner, M.: *Elastic image registration in presence of polyconvex constraints.* Submitted: Proceedings of the International Workshop on Optimal Control in Image Processing, Heidelberg, Germany, May 31 - June 1, 2010

51. [Yezzi/Zollei/Kapur 01] Yezzi, A.; Zollei, L.; Kapur, T.: *A variational framework for joint segmentation and registration.* In: Proceedings of the IEEE Workshop on Mathematical Methods in Biomedical Image Analysis (MMBIA'01). IEEE Computer Society; Washington 2001, 44 – 51

Last modification: 31. 08. 2010

Author's address: Marcus Wagner, University of Graz, Institute for Mathematics and Scientific Computing, Heinrichstraße 36, A-8010 Graz, Austria.

Homepage / e-mail: `www.thecitytocome.de` / `marcus.wagner@uni-graz.at`